DEPARTMENT OF PHYSICS, UNIVERSITY OF JYVÄSKYLÄ
RESEARCH REPORT No. 3/86

ION GUIDE METHOD FOR ISOTOPE SEPARATOR

BY
JUHA ÄRJE

Academic Dissertation
for the Degree of
Doctor of Philosophy

To be presented, by permission of the
Faculty of Mathematics and Natural Sciences of the
University of Jyväskylä,
for public examination in Auditorium S-212 of the
University of Jyväskylä on August 2, 1986,
at 12 o'clock noon

Jyväskylä, Finland
July 1986

URN:ISBN:978-951-39-8546-2
ISBN 978-951-39-8546-2 (PDF)
ISSN 0075-465X

2. p.

Jyväskylä, Jyväskylän yliopisto, 2021

Preface

This study was done during the years 1978-1985 mainly at the Department of Physics, University of Jyväskylä. Some of the measurements were carried out at the Cyclotron and Radioisotope Center, Tohoku University in Sendai, Japan. I would like to thank these laboratories for the excellent working conditions.

I am indebted to numerous people for their support in the course of this whole project. Special appreciations are extended to my teachers, Professor K. Valli and Dr. J. Äystö. Professor K. Valli initiated this project and the first successful part of the ion guide development with a radioactive source was done in a close co-operation with him. In the next stage of the project the ion guide was connected on-line to the cyclotron. For that development, a relatively large group of investigators and technicians was formed. The group was successfully lead by Dr. J. Äystö. I would like to take the opportunity to thank also the other members of the group for their intensive and enthusiastic co-operation, Mr. P. Taskinen, M.Sc., Mr. A. Hautojärvi, Lic.Phil., Mr. K. Vierinen, Lic.Phil., Dr. J. Honkanen, Mr. H. Hyvönen, M.Sc., and Miss V. Koponen, M.Sc. Without excellent technical support this work would be impossible and so I am very indebted to Mr. V-M. Helenius, engineer, Mr. H. Leinonen, technician, and to the staff of the machine shop, Mr. A. Lyhty, Mr. P. Onkila and Mr. E. Liimatainen.

I am indebted to Professors T. Åberg and R. Nieminen and to Dr. J. Timonen for valuable discussions with them concerning the atomic physical processes in the ion guide. I am obliged to Professor J. Hattula for fruitful discussions about this thesis.

I wish Professor M. Fujioka and his group every success with the ion guide in their ISOL system. At the same time I also would like to thank him and Dr. T. Shinozuka and Dr. M. Yoshii for the opportunity to collaborate with them in the developing work of the ion guide in Sendai during the spring 1985.

I also wish Professor R. Coussement and his group from the Instituut voor Kern- en Stralingsfysika, Katholieke Universiteit in Leuven, Belgium and Professor T. Nomura and his group from the Institute for Nuclear Study, University of Tokyo, Japan for much success with the ion guide method they have chosen for their ISOL systems which are connected to heavy ion accelerators. I also would like to thank Professor R. Coussement, Dr. M. Huyse and Miss K. Deneffe, M.Sc. for the opportunity to collaborate with them and to gain experience with their ion guide during summer 1985.

I am obliged to Mr. P. Rötkönen and Mrs. M. Lahtinen for carefully finished drawings and to Dr. C. Parry for revising the language of the manuscript of this thesis.

Finally I wish to express my most sincere thanks to my wife Pirkko-Liisa and to my sons Matias, Johannes and Aleksis for their patience, support and encouragement throughout my work.

For financial support I am indepted to the Academy of Finland, to the Emil Aaltonen Foundation and to the University of Jyväskylä.

Jyväskylä, June 1986

Juha Ärje

ION GUIDE METHOD FOR ISOTOPE SEPARATOR

Abstract

A fundamentally new ISOL technique, the ion guide method for isotope separator has been developed. The method is based on thermalization of primary recoil ions from nuclear reactions or radioactive decays in helium and on their transfer by helium flow through a differential pumping system into the accelerating stage of an isotope separator. With this approach, separation times in the submillisecond region are achievable for both volatile and nonvolatile elements. Three main differences between the ion guide and conventional ion sources are emphasized: In the ion guide no ionizers are used, instead natural charge creation mechanisms related to nuclear reactions and radioactive decays are exploited. Secondly, the operation takes place at room temperature and thirdly the simple construction has no wearing components. These properties ensure continuously stable working conditions.

The number of recoils per unit reaction cross-section stopped in helium seems to be almost constant in different reactions when equal operating conditions are used. The overall separation efficiencies measured for heavy nuclides induced in light ion reactions are up to 10%. The shortest lived activity identified in an on-line separation is the 182 μs isomeric state of ^{207}Bi.

CONTENTS

1. INTRODUCTION

Recent progress in studies of exotic nuclides far off beta stability [1-3] is largely due to the rapid development of on-line mass analyzing devices and especially of ion sources therein. On-line isotope separators (ISOL) equipped with fast and efficient ion sources have played a central role in discoveries and studies of several new nuclear properties of highly unstable nuclei [2-4]. The isotope ^{32}Ar which is one of the rare known nuclei with a proton excess Z-N of four, gives an idea of the difficulties encountered in separation techniques: This short-lived ($T_{1/2}$= 98 ms) isotope is induced from vanadium by high energy protons. With a proton beam intensity of 1μA the production rate of unwanted radioactive atoms from the target is as high as ≈10^{13} atoms/s, while the yield of ^{32}Ar is only ≈500 atoms/s [5].

In most ISOL systems of today [6], the target is an integral part of the ion source. The recoiling reaction products are imbedded in the surrounding material or they are collected by a catcher from where they are driven out by thermal diffusion at high temperature. The next step in the process is ionization of the radioactive products. After ionization by energetic electrons the recoils are ready for mass analysis. The main demands of the ISOL process, a high efficiency of ionization (≈>1%) and versatility, i.e. ionization of almost all elements, have already been reached by these techniques [7]. However, there is still a serious problem with a long delay time which is caused by the slow release of nonvolatile elements from the catcher or from the stopping material in the ion source. At present, the integrated target-chamber ion source systems are effective for nuclides having half-lives ≈>0.5 s and melting points ≈<1000 °C [6]. As far as is known, there are only few exceptions to these limits [8-11]. It should be emphasized that almost half of all natural elements (=43) have a melting point above 1000 °C and thus their most short-lived nuclides have not been within reach of these techniques.

One solution to reduce the longest delay times is the use of a helium-jet coupled ion source. There energetic recoil particles are thermalized in

high pressure helium (1-2 bar) and are transported with helium flow through a long capillary into the ion source [12-17]. The step that depends on thermal diffusion from the solid stopping material is eliminated, but the reionization of recoils is necessary. With a several meters long capillary and a small target chamber it has been possible to study the refractory ^{24}Si which has a half-life of ≈100 ms [18]. Overall efficiencies up to a few per cent have been reached with these techniques.

In this thesis, a fundamentally new ISOL technique, the ion guide method for isotope separation, is introduced. The ion guide permits primary recoil ions produced in nuclear reactions or in radioactive decay to be passed directly through an isotope separator, without a conventional ion source. The idea of separating primary ions from reactions or decays is not new [19-21], but after a few earlier attempts it has now been realized for the first time in on-line conditions. The ion guide has been under development now for seven years. The first version worked off-line using a radioactive recoil source [22,23]. After a satisfactory operation off-line, the system (IGIS, Ion Guide Isotope Separator) was connected on-line (IGISOL, Ion Guide Isotope Separator On-Line) to the cyclotron at the Department of Physics, University of Jyväskylä three years ago [24-26].

The ion guide is based on the helium-jet technique with a modified target chamber to provide recoil ions. Two main differences between the ion guide and conventional ion sources are apparent: In the ion guide method no ionizers are used; instead natural charge creation mechanisms inherent in nuclear reactions and stopping processes are exploited. These mechanisms create in helium singly charged atomic recoil ions and permit them to be injected directly into an isotope separator. The second difference is the operation at room temperature. This together with a simplified construction gives a continuous stability in operation. With this approach, separation times and efficiencies are independent of the volatility of the element which means that the very fast on-line mass separation is now extended up to the most refractory elements [25].

The second section of this thesis describes various charge creation mechanisms that can be expected during nuclear reactions and radioactive decay, as well as during penetration of energetic recoils through the target material and finally during their thermalization in the helium buffer gas. Also a description is given for survival and motion of the thermalized recoil ions in the flowing helium. Experimental conditions in on-line operation differ from those prevalent off-line in two main respects: A plasma is created in helium by a projectile beam and recoil ranges are usually much longer from reactions than from a radioactive α-source.

After the first successful experiments the development of the ion guide has concentrated on increasing its efficiency. The main differences in the present on-line system as compared to the first off-line version are a higher throughput of helium and a shorter evacuation time of the target chamber. The experience of several years has shown that in addition to experiments with the accelerator, also experiments off-line are still useful in a further development of the system. At present there are two kinds of sources to provide ions for off-line test experiments. In addition to the α-active ^{227}Ac recoil source, a spark discharge ion source to produce stable atomic and molecular ions has been found useful in simulating many features of on-line transportation and in tuning the isotope separator.

The first chapter of the third section describes the construction of the ion guide and its operating principle, including also the pumping system and the calculated transport parameters. The second chapter introduces the off-line measurements. Following the description of the spark discharge ion source and results obtained with it, the basic development of the ion guide carried out with the ^{227}Ac recoil source is presented in detail. The last part of this section concentrates on the ion guide in on-line operation. In addition to the measurements with the IGISOL at the University of Jyväskylä, some results measured with the Tohoku IGISOL at the Tohoku University in Sendai, Japan [27] are included.

2. PHYSICAL BASIS OF THE ION GUIDE METHOD

The ion guide method for an isotope separator permits thermalized recoils produced in nuclear reactions or emitted from a radioactive source to be mass separated directly as primary ions. The use of primary ions is based on charge creation and reset mechanisms associated with nuclear reactions and radioactive decays and with thermalization processes of recoil particles in a high-pressure buffer gas.

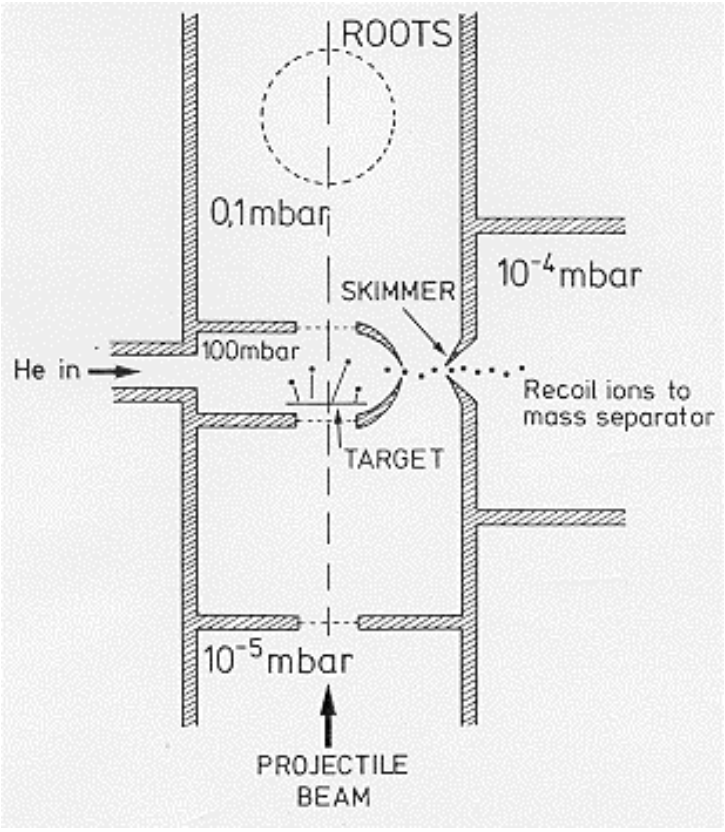

Fig. 2-1. Operating principle of the ion guide.

A schematic drawing of the ion guide and its operating principle is shown in fig. 2-1. The main points in the operation are the following: Immediately, after the reaction or decay products are thermalized in a gas phase in the helium-filled target chamber, they are swept along with

helium through an exit hole or a capillary into an adjacent vacuum chamber. Helium is removed from the vacuum chamber by means of a high-speed Roots blower while the positive recoil ions are guided by an electric field through a skimmer hole into the accelerating section of the separator.

2.1. *Charge creation and survival of recoil ions*

The following presentation of atomic and ionic processes in the ion guide is based on an extensive literature survey. The most relevant processes are identified and described qualitatively. Comparisons are made to measurements which correspond to the situation in the ion guide. As far as is known, quantitative investigations of atomic processes as they appear in actual ion guide operation have not yet been made. Further, exact calculations from different theories would be extremely complicated, because many kinds of atomic and molecular processes take place at the same time in the target chamber.

2.1.1. Initial charge creation - highly charged ions

A high initial charge state ($q>+2$) for a recoil can be produced via ionization in collision processes connected with a nuclear reaction or radioactive decay. Three different mechanisms can be distinguished: The first is an inner-shell vacancy production in collisions between a projectile and target atoms. Inner-shell vacancy production by protons and alpha particles is well understood by models in which the effect of these ions on atomic systems is considered to be a perturbation by a point charge [28]. A universal curve of the ionization cross-sections, based both on theory and experiments, reaches its maximum value when the velocity of a light ion projectile is near the velocity of the orbital electron of the target atom. This is roughly true for any electron shell.

Theoretical cross-sections of K- and L-shell ionizations in all elements induced by protons and by He-ions [29] reveal that vacancy

production in the K-shell is very small for all elements, when proton energies of 15-20 MeV or ^{3}He- and α-energies of 15-27 MeV are used. The cross-sections are ≈10^{-20} cm^2 for light and ≈10^{-24} cm^2 for heavy targets. However, for light targets, ionizations of L-shells are notable. For example, in the reactions ^{46}Ti(p,n)^{46}V with 15.4 MeV protons and ^{40}Ca(^{3}He, α)^{39}Ca with 15 MeV ^{3}He, studied in the present work, the calculated probabilities of L-shell ionization of recoil atoms are 0.12 and 1.0 per nuclear reaction, respectively. Furthermore this type of ionization mechanism is important for heavier target atoms from their outer electron shells, as can be deduced from a comparison of the velocities of the orbital electrons to the used velocities of the projectiles.

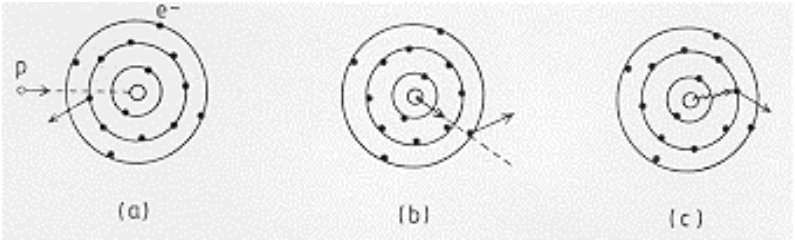

Fig. 2-2. Initial charge creation of recoil in a nuclear reaction or in radioactive decay.
(a) Ionization caused by an incoming projectile.
(b) Ionization following emission of a charged particle from a compound nucleus or in radioactive decay.
(c) Ionization via de-excitation of a highly excited nucleus.

The second ionization mechanism is related to the decay of a highly excited nucleus by emitting charged particles, which can be considered as inner projectiles. During the process of a nuclear reaction an excited compound nucleus decays by the emission of one or several particles. An emission of a charged particle can induce a perturbation into the electronic structure of the decaying atom. This can result in the electronic excitation or ionization of the atom [30-32]. If the velocity of an emitting particle is low compared to velocities of orbital electrons, the change in the electrostatic field between the nucleus and the electron shells is relatively slow, i.e. adiabatic. This means that the probability for an inner-shell ionization is small. The ionization in these shells is mainly

caused by a Coulomb ejection. This processs also occurs in radioactive decay. For example, in the α-decay of ^{210}Po the ionization probabilities for K-, L- and M-shells are $2x10^{-6}$, $6x10^{-4}$ and $2x10^{-2}$, respectively [33]. The situation is different when an emitting particle is fast. This type of a non-adiabatic emission of a particle causes an electron shake-off effect [34] with a high probability of an electron emission from an atom.

The probability that at least one orbital electron is detached from the recoil atom ^{133}Cs in ß-decay of the ^{133}Xe, is measured to be ≈0.2 [35]. In the α-decay, the departure of the α-particle constitutes a sudden perturbation for the outermost electrons, and consequently there is a high probability that one or more electrons will be ejected [36].

Similar processes leading to charged recoil atoms in nuclear disintegrations have also been found in fission, in K-capture and in neutron emission [32]. Quantitative values of probabilities can be found in few cases only [33,37 and references therein].

The third mechanism producing charged recoils after a nuclear reaction or radioactive decay is nuclear internal conversion. Internal conversion, where an excitation energy or part of it is transferred directly to an electron orbiting the nucleus, is a common phenomenon in the de-excitation processes of heavy nuclei.

In all ionization mechanisms, one or more electron shell vacancies produced, are filled by electrons from outer orbitals. The energy difference is either released by the emission of photon radiation or transferred to another outer shell electron which subsequently will be excited or emitted from the atom as an Auger electron. For a K-shell vacancy the Auger electron emission dominates for those elements whose atomic number Z<32 and for the M, N and the higher shells throughout the range of the elements [38]. The Auger transition generates vacancy cascade and converts the atom into a highly charged ion [39].

Figure 2-3 presents the charge state distribution of recoils ^{222}Ra after α-decays in the ^{226}Th. About 75% decay to the ground state and 23% to the excited state 111 keV, which de-excites via internal conversion (>95%). In the former case charged recoils may be created via stripping of recoils when leaving the platinum backing plate (ch. 2.1.2)

and in internal ionization during the α-decays. In the latter case additional ionization of recoils is caused by Auger cascade after the internal conversion. The final result of the processes is that about 80 per cent of the recoils are ionized.

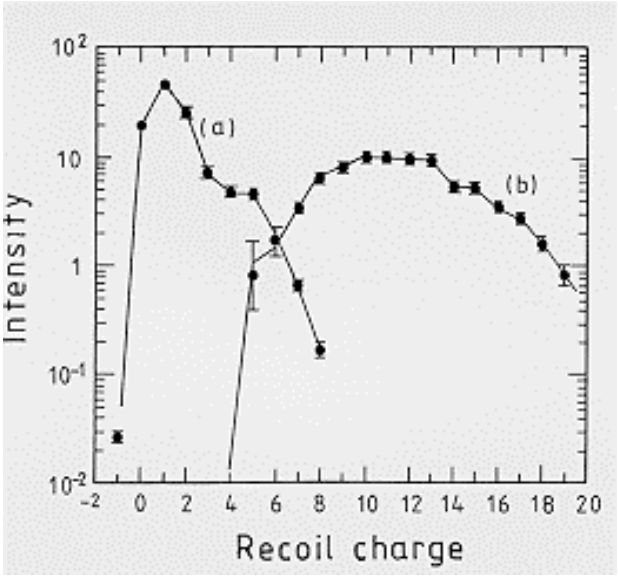

Fig. 2-3. Charge state distributions of recoils ^{222}Ra following the α-decay of ^{226}Th.
(a) Recoils from decays to the ground state,
(b) recoils from decays to the excited states that de-excite via internal conversion. [40]

Typically lifetimes of nuclear excitations are of the order of 10^{-12} s or more and Auger cascade takes place within 10^{-15} s [41]. It follows that in consequtive conversions, at least the innermost electron shells have time enough for rearrangement before the next conversion. This means that in such cases independent Auger cascades still increase the charge states of the recoils. The average charge state of the ^{223}Ra recoil ion has been found to be q≈+25 after 3 consequtive converted transitions in the α-decay of ^{227}Th [42].

As an example from the present study, the isotopes ^{219}Rn, ^{215}Po and ^{211}Pb, emitted in α-decay chain of the ^{227}Ac, were mass separated as

primary ions. Only 0.85% of the ^{219}Rn isotopes are initially in the ground state. Over 95% of the low-lying excited states de-excite via internal conversion. On the basis of this it can be assumed that a significant part of ^{219}Rn recoils are initially highly charged ions. On the other hand, 81% of ^{215}Po and over 99% of ^{211}Pb isotopes are produced in their ground states [43]. Their ionization is believed to be partly due to internal ionization and partly due to stripping during their thermalization in helium buffer gas.

As an example of the on-line mass separation, in the reaction ^{40}Ca(^{3}He, α), the recoil ^{39}Ca having an electron vacancy in the L-shell, would have an average charge state q≈+2 after the Auger effect [41].

2.1.2. Electron loss in solid targets and in helium buffer gas

After a nuclear reaction or radioactive decay, fast moving recoil particles change their charge states continuously while passing through target material or penetrating into buffer gas. Each collision between the recoil and the target atom has a certain probability for loss and capture of electrons. Statistical competition between loss and capture in many successive collisions will then produce a certain distribution of charge states for ions having the same energy. When the number of collisions becomes sufficiently large the distribution will reach an equilibrium. The resulting equilibrium charge state distribution, which is gaussian-like, depends on ion velocity V_i, ion species Z_i and target species Z_t, but is independent of the initial charge state composition of the recoil ions [44,45]. It must be added that energy loss in a thick target reduces the ion velocity and thus gives rise to changes of the equilibrium charge state distribution. This effect becomes significant for the target thicknesses which grossly exceed the minimum thickness needed to produce the equilibrium. Since charge changing cross-sections are large (≈10^{-15} cm^2), the penetration of ≈1 μg/cm^2 for an ion in the target material is enough to produce the charge state equilibrium for slow recoil ions.

Interactions between charged recoils and matter are extremely complicated and difficult to predict: No quantitative theory is available

for average equilibrium charge states. However, there are some semiempirical relations for the average charge states and the charge state distributions of ions with velocities $V_i \approx > v_o$ ($v_o = 2.19 \times 10^8$ cm/s, the first Bohr orbital velocity).

A semiempirical formula [46] for average equilibrium charge state in solids is

$$\bar{q} = Z_i [1 + (0.61 Z_i^{-a} V_i/v_o)^{-1/k}]^{-k} , \qquad (2.1)$$

where a=0.45, k=0.6 and $V_i > v_o$. The effect of the target material itself on the charge states is so small that the dependence on the target Z_t has been excluded. The width of the equilibrium charge state distribution is given by

$$d = 0.5 \{ \bar{q} [1 - (\bar{q}/Z_i)^{1/k}] \}^{1/2} . \qquad (2.2)$$

In eq. 2.1 deviations of q from experimental values do not exceed 5% and in eq. 2.2 deviations of d are within ≈20% for ions $Z_i \approx > 20$ [46]. Thus, these equations offer a useful way of estimating the average charges of ions emerging from solids (fig. 2-4a).

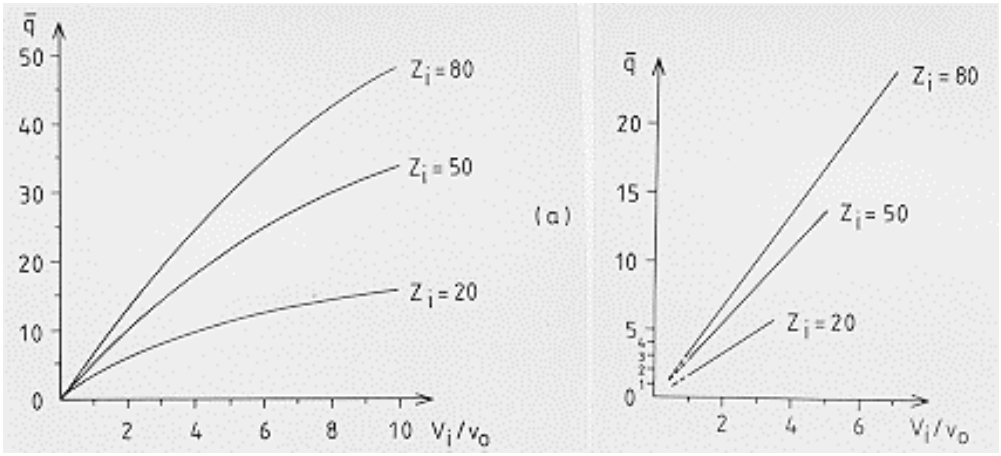

Fig. 2-4. Average charge states of recoil ions with Z_i= 20, 50 and 80 as a function of the ion velocity when travelling in a solid material (left) or in a gas (right). $V_i/v_o = 0.2 (E/A)^{1/2}$, where [E/A]= keV/u.

An often used expression for the average equilibrium charge state of an ion penetrating into a gas is

$$q = A\ Z_i^{1/2}\ V_i/v_o\ , \qquad (2.3)$$

where A is ≈0.39 and $q \approx < 0.3Z_i$ [45]. Also in this case it has to be noticed that the equation is applicable for a rough estimate of the charge only (fig. 2-4b). Especially it underestimates average charge states at lower ion velocities ($V_i < v_o$) in helium.

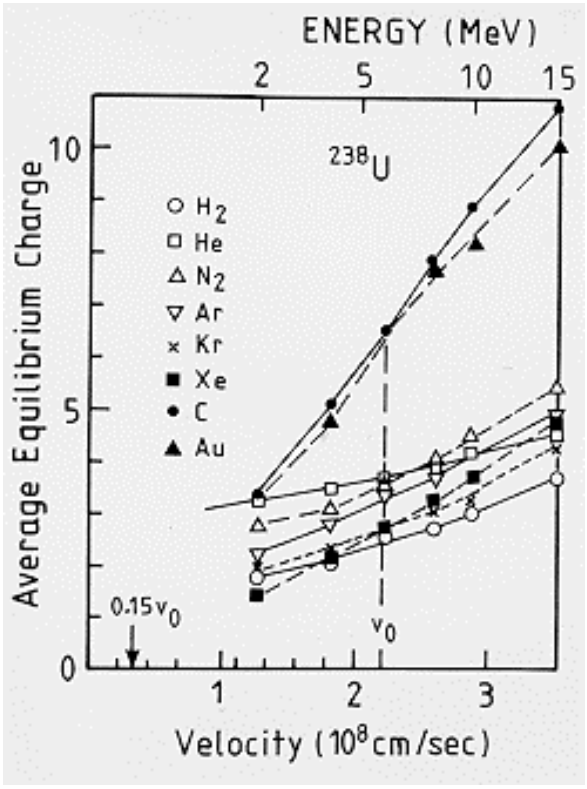

Fig. 2-5. Average equilibrium charge state as a function of energy for ^{238}U ions passing through gases and solids, measured by Wittkower and Betz. [48]

No theoretical and only few experimental data about charge states of ions penetrating into solids and gases exist at small ion velocities

($V_i < 0.5v_o$). For example, it has been found experimentally that the average charge states of Pr, Gd and Lu ions are $q \approx +1.5$ after passage through a thin carbon foil (4 μg/cm^2) with the velocity $V_i \approx 0.25v_o$. Under the same conditions, the average charge states for heavier ions Hg, Tl and Pb are $q \approx +0.7$ with $V_i \approx 0.20v_o$, consisting of approximately one half of +1-charged ions and of the other half of neutrals and +2-charged ions [47].

Generally a striking difference between charge state distributions in gases and solids at velocities $V_i \approx > v_o$ is that solids lead to a higher charge state [44].

Helium is a special case as a stripping medium [48-50]. For very high velocity ions it is the least efficient stripper, but at low velocities $V_i \approx < 0.6v_o$, it is the most effective among both solid and gaseous strippers (fig. 2-5). A possible explanation for this is that for helium the orbital velocities of its electrons ($v_e \approx 1.4v_o$) are relatively higher than the ion velocities, whereas this is not so for other strippers. Thus it appears that ions with relatively low velocities and with low charge states cannot transfer sufficient energy to a helium atom to liberate one of its electrons. This leads to a significantly reduced capture cross-section [48].

Recoil energies of the recoil products from the ^{227}Ac source are around 100 keV which corresponds to the velocities of $\approx < 0.14v_o$. At this velocity region ionization of recoils via stripping in solid source material seems to play a minor role (fig. 2-4a). An energetically similar situation occurred for the recoils from the reaction ^{207}Pb(p,n)^{207}Bi with the proton energy of 20 MeV; the estimated average charge state of the recoil in the target is below +1. On the other hand, in the reaction ^{24}Mg(^{3}He,2n)^{25}Si with the bombarding energy of 27 MeV, the calculated velocities of recoil ions are $V_i \approx 2.2v_o$ and the corresponding average charge state $q \approx +5$ in the target. The recoil velocities in all other reactions studied in this work were between $0.14 \approx < V_i/v_o < 2.2$ and the calculated average charge states $0 < q \approx < +5$.

The highest velocities of recoils that can be thermalized in helium in the present ion guide are $V_i(\max) \approx 0.25v_o$ for light, and $\approx 0.20v_o$ for heavy recoils (fig. 2-9). At these velocities the experimental results

[48,51,52] indicate that +1 is a dominating charge of ions in helium. For example, for 40 keV Ar ions ($V_i=0.20v_o$) the following fractions of charge states have been measured in helium; 5%, 89% and 6% for charges 0, +1 and +2, respectively [49]. Referring to those results, it seems evident that in the case of neutral recoils emerging from the target, the stripping in the beginning of recoil thermalization in helium can still ionize some of them.

2.1.3. Electron capture of energetic recoil ions in helium

The charge state q of a reaction or decay product, penetrating into helium buffer gas, can be anything between $0 \le q \le q_{max}$. The charge state depends on the early history of the recoil, mainly on its recoil energy and its initial position in the target. Low charge states are likely for recoils coming from deep inside the target. On the other hand, the recoils emitted from the surface of the target may have a very high charge.

During stopping process in high pressure gas the charge states of highly charged recoil ions are reduced in asymmetric electron capture processes between ions and He atoms,

$$R^{q+} + He \rightarrow R^{(q-1)+} + He^{+} . \qquad (2.4)$$

In eq. 2.4 an energetic ($E_i > 0.1$ eV) recoil ion R of charge +qe picks up one of the atomic electrons during collision with a neutral He atom, thereby emerging with a charge +(q-1)e. A number of theoretical investigations of such electron capture have been made for medium- to high-velocity, highly charged (q>+2) ions colliding with atoms [53]. However, due to the complexity of the three-body interaction in the capture process, it has been possible to perform ab initio calculations only for the simplest collision systems and only for limited ranges of the physical parameters involved.

Universal scaling of the capture cross-sections for energetic highly charged ions in gases shows that for recoil ions with scaled energy

$E_i/(A_i q^{4/7}) \approx < 16$ keV/u the cross-section over charge has a constant value $\sigma_c/q \approx 2.3 \times 10^{-16}$ cm^2. This cross-section agrees well with experimental results of one electron capture reactions, if the following two requirements are satisfied: $q > +4$ and $2q/(V_i/v_o) \gg 1$ [54].

There is no common theory to predict the dependence of the capture cross-section on the ionic charge q, the nuclear charge Z_i and on the collision energy when the charge state of an energetic ion is $q \leq +4$. However, plenty of experimental data from 1 keV to a few tens of keV exists [55-58]. Almost all the experimental data shows a monotonic dependence of the cross-sections on q. But there is also experimental evidence that in some collisions cross-sections do not change monotonically but that some maxima and minima exist [59].

The energy dependence of the experimental cross-sections below energies of 25 keV/u ($V_i = v_o$) generally seems to be very small [60]. Also some theories developed for special cases predict the cross-sections to be independent of the energy [54,61-63]. However, in some cases the energy dependence of the reaction has been found to be strong: Experimental one electron capture cross-sections in helium for low energy boron and carbon ions, having initial charge states of q=+4 and +3 and ion velocities of $V_i \approx 0.1\text{-}0.2\ v_o$, are $\sigma_c(4 \rightarrow 3) \approx 10^{-16}$ cm^2 and $\sigma_c(3 \rightarrow 2) \approx 10^{-15}$ cm^2. The cross-section $\sigma_c(4 \rightarrow 3)$ is strongly dependent on the collision energy, being 5-10 times higher than the above value at the velocity $V_i \approx 0.45 v_o$ [59].

From the experimental data it can be noticed that the capture cross-section of an ion decreases when the ionization potential of the gas atom increases. For example in the reaction

$$Xe^{2+} + X \rightarrow Xe^{+} + X^{+}, \qquad (2.5)$$

the capture cross-sections for 30 keV Xe^{2+}-ions ($V_i \approx 0.1 v_o$) are $\approx 2 \times 10^{-15}$ cm^2, $\approx 7 \times 10^{-17}$ cm^2 and $\approx 1 \times 10^{-17}$ cm^2 when X is Ar, Ne and He, respectively. In the same buffer gas the capture cross-sections of different ions have almost the same value [64]. It can be concluded that

one electron capture cross-sections of ions, having charge states $+2 \leq q \leq +4$ and velocities $V_i \approx < v_o$ in helium, are $\sigma_c \approx 10^{-15} - 10^{-17}$ cm^2.

In the charge-exchange reaction,

$$R^+ + He \rightarrow R + He^+ + \Delta E , \qquad (2.6)$$

an energetic +1-charged ion R^+ collides with a helium atom and becomes neutral. The energy defect ΔE is defined as

$$\Delta E = E_I - E_F , \qquad (2.7)$$

where E_I is the initial and E_F the final total internal energy of the colliding system. For the capture from and into ground states ΔE is given by the difference in ionization potentials of R and He. Neutralization reactions like the one given in eq. 2.6, obey the so-called "adiabatic maximum rule" [65]. According to this the capture reaction reaches its maximum cross-section when collision time ($\approx a/V_i$, a=atomic dimension) is comparable to an electron's transfer time ($h/\Delta E$, h= Planck constant). Thus the ion velocity corresponding to the maximum cross-section should then be

$$V_i(\sigma_{c,max}) \approx a \ \Delta E/h . \qquad (2.8)$$

The relation 2.8 describes reasonably well a large number of reactions like 2.6 with the adiabatic parameter $a=7 \times 10^{-8}$ cm [66].

The velocity region $V_i < V_i(\sigma_{c,max})$ is termed the adiabatic region; when the collision velocity decreases the capture cross-section falls off rapidly. Finally, the collision takes place so slowly that the adiabatic adjustment of an atom into the perturbation caused by an ion is likely without an electronic transition being involved. In the adiabatic velocity region there are no reliable theories for calculation of electron capture cross-sections in the neutralization reaction 2.6. For experimental results it must be referred to the electron loss measurements (ch. 2.1.2), which showed that the charge +1 is dominating in helium in the velocity region $V_i \approx < v_o$.

Considering the neutralization of an energetic recoil ion in the present ion guide, via the electron capture from a helium atom, the following things should be noticed: The ionization potentials of the studied recoils are typically 6-8 eV. According to eq. 2.8 these values give maximum capture cross-sections at velocities $V_i \approx$ 1.3-1.4 v_o in helium. Recoils with so high velocities in the buffer gas are lost to the walls of the target chamber. Recoils are thermalized in the gas phase, when the velocities are at most $V_i \approx$ 0.20-0.25 v_o. This is exactly the adiabatic velocity region where the recoil neutralization in collisions with helium atoms is expected to be unimportant.

2.1.4. Electron capture of thermal recoil ions in helium - the role of impurity molecules

Due to different charge creation mechanisms of recoil ions in the ion guide, the velocity distribution of +2- and +1-charged recoils in helium may extend from the highest velocities ($V_i \approx 0.25 v_o$) down to the thermal ones, $V_i \approx 10^{-4} v_o$.

At the region of thermal or near thermal energies ($E_i \approx < 0.1$ eV) the interacting particles are relatively far away from each other during a collision. In the charge transfer reaction

$$R^{2+} + X \rightarrow R^{+} + X^{+} , \qquad (2.9)$$

where X is an atom or a molecule, the initial state of the collision is slightly attractive ($\propto r^{-4}$, r= internuclear separation) because of the polarization of the atom or molecule induced by the ion. The final state, conversely, is strongly repulsive due to a Coulomb repulsion ($\propto r^{-1}$) between two positively charged ions (fig. 2-6).

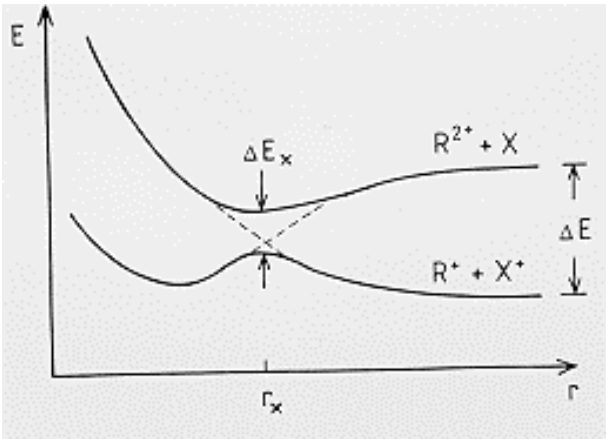

Fig. 2-6. Pseudocrossing of potential energy curves for the process $R^{2+} + X \rightarrow R^{+} + X^{+} + \Delta E$.

When the ion comes close enough particles form a quasimolecule for which the potential energy is dependent on the internuclear separation r. The electron transfer is a transfer between the two energy states of the quasimolecule in the region of separation r_x, where the potential energy curves approach and pseudo-cross each other. The effective energy defect ΔE_x near r_x may be remarkably less than the energy defect ΔE between the separated ion and the neutral particle. Exceptionally large transfer cross-sections in the region of low collision energies are to be expected [64,68-70]. Hasted et al. and Olson et al. have theoretically [71,72] shown that the charge transfer is most probable in the crossing point of the potential curves at the distance

$$r_x = 14.4 / \Delta E , \qquad (2.10)$$

where the units are 10^{-10} m and eV, respectively. Many experimental results show that the charge transfer for +2-charged ions in gases is very probable at distances $0.25 \approx< r_x \approx< 0.7$ nm, i.e. with the energy defects $2 \approx< \Delta E \approx< 6$ eV. The corresponding rate coefficients of the transfer reactions are $\alpha_c \approx< 10^{-9}$ cm^3/s [73], which give the maximum cross-sections of the order of 10^{-13} cm^2 at thermal velocities. Outside the thermal energy region the rate coefficients decrease dramatically.

As an example of the sensitivity of the thermal charge transfer reactions the rate coefficients of Ar^{2+} with various atoms and molecules are shown as a function of internuclear separation in fig. 2-7. According to Lindinger the exoergicity ($\Delta E>0$) of the reaction rather than the nature of the ions appears to determine the reaction rate. Reactions are almost always fast when neutral reactants are molecules. Because of the high density of energy states in molecules (electron-, vibration- and rotation states) there is almost always a crossing at a suitable distance for potential energy curves of initial and final states [73].

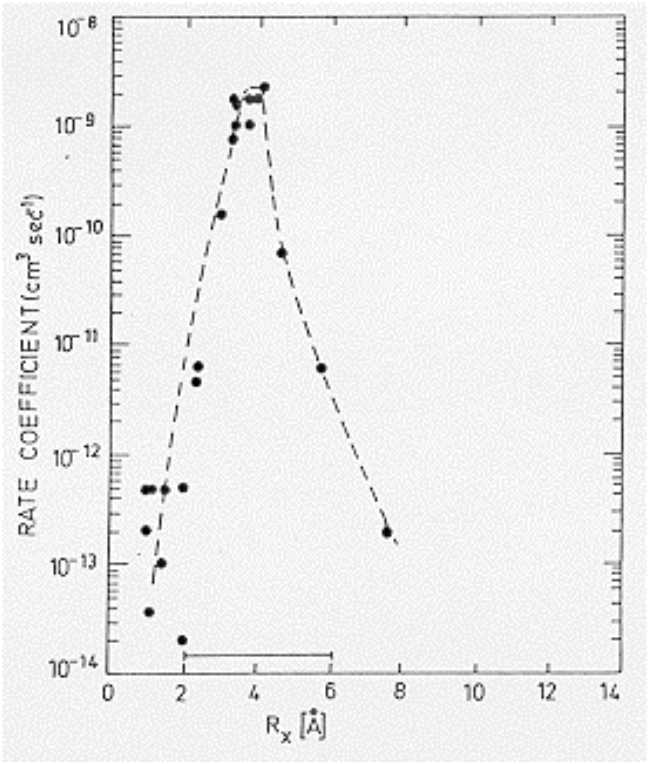

Fig. 2-7. Rate coefficients of the reaction of Ar^{2+} with various atoms and molecules as a function of the internuclear separation. Data collected by W. Lindinger. [73]

For thermal or near thermal recoil ions with low charge, the asymmetric charge transfer reactions in helium

$$R^{q+} + He \rightarrow R^{(q-1)+} + He^{+} + \Delta E\,, \qquad (2.4)$$

where the recoil R has a charge state of q=+2 or +1, seem to be improbable. The reason is the strong endoergicity of such reactions. Only few elements have a second ionization potential higher than the first ionization potential of helium. But the situation is different, if small amounts of impurity molecules, such as H_2O, N_2, O_2, etc., are mixed in the helium.

In the ion guide the concentration of impurities in helium is about 100 ppm and the main components are the ones mentioned. The ionization potentials of the impurity molecules are typically 10 to 16 eV, being between the first and the second ionization potentials of recoil ions. The charge transfer reactions

$$R^{2+} + M \rightarrow R^{+} + M^{+} + \Delta E\,, \qquad (2.11)$$

where M is an impurity molecule, are very favourable as exoergic reactions. The calculated probabilities in the ion guide for reactions like 2.11 are few tens of per cents if $\Delta E \approx 4$ eV. On the other hand, in the same energy region the neutralization reactions

$$R^{+} + M \rightarrow R + M^{+} + \Delta E \qquad (2.12)$$

are very unlikely. Because of the endoergicity of such reactions, the cross-sections are in orders of magnitude smaller than in the reaction 2.11 [73]. Finally, it must be added that excited ions and molecules may make the processes much more complicated [74].

2.1.5. Recombination, reionization and clustering of thermalized recoil ions

When a radioactive recoil source is used, or if one operates with the cyclotron beam induced activity, free electrons are always present in the buffer gas. The electron densities differ greatly in these two cases. In off-line conditions, when using the ^{227}Ac source with the activity of $\approx 7 \times 10^5$ Bq, the degree of ionization or plasma density of the buffer gas is

estimated to be less than 10^{-10} at the pressure of 200 mbar. In the case of the 20 MeV proton beam with the intensity of 1 μA, the plasma density is estimated to be of the order of 10^{-7}. An approximately ten times higher degree of ionization is caused by the α-beam with the same energy and current. In on-line conditions the estimates are based on energy losses of the projectile particles in 100 mbar helium, including an additional ionization induced by secondary electrons emitted from the target, buffer gas and from the windows of the target chamber [75,76]. In the case of the proton induced plasma, the value of the degree of ionization conforms well with that calculated with the experimental value of the ionization cross-section of protons in helium [77].

The following recombination reactions between thermalized recoil ions (R^+) and free electrons or negative molecular ions (M^-) are most likely in the buffer gas:

$$\begin{aligned} &\text{(a)} \quad R^+ + e^- + He \rightarrow R + He \\ &\text{(b)} \quad R^+ + M^- + He \rightarrow RM + He\,. \end{aligned} \qquad (2.13)$$

Because of the relatively low degree of ionization in off-line operation with the radioactive source, the conditions do not fulfill the criteria for plasmas [78], and reactions like 2.13 are not believed to take place in a notable degree during the transportation of recoil ions out of the target chamber.

In on-line conditions, however, a plasma is present in the target chamber. In the plasma an equal number of positively and negatively charged particles are needed to keep it in electrical balance. The ion guide plasma consists mainly of He^+ and He_2^+ ions and electrons [79]. The plasma decays through three-body recombinations between slow electrons and He ions [80,81], and through ambipolar diffusion of charged particles to the chamber walls. Dielectronic recombinations of helium ions are not likely in such a weak plasma. A steady state of the plasma is maintained by continuous ionization induced by the projectile beam.

The following densities of particles, shown in table 2-1, are estimated to be present in the target chamber in typical on-line conditions (ch. 3.1.2).

Particle	Density (cm^{-3})	Remark
He	2.5×10^{18}	p_{tc}=100 mbar, T≈293 K
M	$\approx 10^{14}$	partial pressure ≈100 ppm
R	10^4 - 10^6	thermalized recoils Y_d (ch. 2.2)
He^+, He_2^+	10^{11}- 10^{12}	plasma density ≈10^{-7} - 10^{-6} [75,77]
M^+	≈10^8 - 10^9	[77]
R^+	>10^3 - 10^6	overall efficiency (ch. 3.3.5.3)
e^-	10^{11}- 10^{12}	plasma density ≈10^{-7} - 10^{-6}
M^-	≈10^6	attachment cross-sections [80,82]
He*	>10^{11}- 10^{12}	[80,82]

Table 2-1. Calculated concentrations of different particles in the target chamber of the ion guide. The plasma is induced by the 20 MeV and 1 μA proton or alpha beam. M= impurity molecule (H_2O, N_2, O_2,...), R= recoil particle.

The loss of positive ions via three-body recombination takes place according to the formula [78,80],

$$dn_i/dt = -\alpha\, n_e\, n_i\, n_n \,, \qquad (2.15)$$

where α is the recombination rate coefficient and n_e, n_i and n_n are the electron, ion and neutral atom number densities, respectively. The decay of the ion concentration as a function of time, derived from eq. 2.15 is

$$n_i = n_i(0)\, \exp(-\alpha n_e n_n t) \,, \qquad (2.16)$$

where $n_i(0)$ is the concentration at the moment t=0.

In the case of the dissociative recombination of He_2^+ ions with electrons, the rate coefficient $\alpha_r \approx 4 \times 10^{-9}$ cm^3/s has been observed at the helium pressure of 80 mbar [83]. Using that value for the rate coefficient and the plasma density of 10^{-7}, the time scale of the dissociative

recombination of He_2^+ ions in the target chamber of the ion guide is found to be

$$t(He_2^+) \approx 1 \text{ ms.}$$

There is a serious lack of data on the three-body electronic recombination coefficients for atomic ions. A few observations, however, show them to be remarkably smaller than those of the dissociative recombinations, being 10-100 times less [76,84]. This indicates that the probable lifetime of a recoil ion in the ion guide plasma is

$$t(R^+) \approx> 10 \text{ ms.}$$

The thus evaluated lifetimes of the recoil ions against electronic recombination are long, if the lifetimes are compared to average diffusion times of recoil ions to the chamber walls (≈5 ms, ch. 3.1.4), or to their average transport times out of the target chamber (≈1 ms, ch. 3.1.4). Due to the low density of negative ions, the situation in the ionic recombination reaction (eq. 2.13b) is the same: the transportation and diffusion of ions take place in such time scales that recombinations are not likely to happen, although the rate coefficients of the three-body associative recombinations are large, $\alpha_r \approx 10^{-6}$ cm^3/s [85].

In on- and off-line conditions reionizations of neutralized recoils in the target chamber are also possible via the reactions,

$$\begin{aligned} &\text{(a)} \quad R + He^* \rightarrow R^+ + He + e^- \\ &\text{(b)} \quad R + He^+ \rightarrow R^+ + He\,, \end{aligned} \qquad (2.17)$$

if the concentrations of helium metastable atoms or helium ions are large enough. Excited helium atoms are produced at least at the same rate as helium ions. The excitation energies of He(2^3S) and He(2^1S) metastable atoms are 19.8 eV and 20.6 eV, and the lifetimes 0.1 ms and 19.7 ms, respectively. Those energies are high enough to ionize (Penning ionization) any atom except neon, which on the other hand can be ionized

by a He ion with its ionization energy of 24.6 eV. At room temperature the rate coefficients of Penning ionization are 10^{-10} -10^{-9} cm^3/s, as measured by W. Lindinger et al. for few atoms and molecules in helium [86].

The following conclusion can be deduced from comparison of the different particle densities in the helium buffer gas: The three-body recombinations of recoil ions, as well as reionizations of neutral recoils through collisions with helium ions or metastable atoms, are not believed to control noticeably the charge creation and exchange processes involved in the operation of the present ion guide. It seems more likely that a part of the recoils emerging into helium from the target or from the radioactive source are charged particles and the rest of them are neutral. Some of the ions are lost during transportation before leaving the chamber - most probably because of their recombinations on the chamber walls due to rapid diffusion.

In certain conditions loss of atomic recoil ions is possible via clustering reactions between recoil ions and impurities of the buffer gas. Molecular clustering of ions is known to occur in gases exposed to ionizing radiation. Because of the large permanent dipole moment, especially H_2O molecules may readily be associated with positive ions to form clustered ions of the type,

$$R^+(H_2O)_n \quad , \quad n \approx< 10.$$

It has been found that the hydration of ions is equal to the partial pressure of neutral water in a buffer gas. Cross-sections for association reactions are not sensitive to the type of buffer gas but they vary strongly inversely to the energy of ions. Bondings between ions and molecules are electrostatic or "chemical", depending on the electronic structure of the central ion, as well as on its size [87-89]. Electron exchange is considered characteristic of "chemical" bonding. It must be added that the field of the cluster formation is still poorly known.

In the ion guide experiments with the ^{227}Ac source a weak clustering effect has been found for the decay products ^{211}Pb (fig. 3-15).

Strong clustering can be avoided by reducing the partial pressure of molecules tending to make clustered ions. There is also a feature of the ion guide operation which may prevent an injection of clustered ions into the separator: An extraction of ions by the skimmer voltage at relatively high pressure leads to cluster fragmentation with a high probability - at least in the case of weak electrostatic bondings [84].

2.2. *Ranges of recoils in the target and in helium*

In about two thirds of the nuclear reactions studied here, recoil energies were so low ($E_i/A_i < 12.5$ keV/u) that their range information are not included in the tables of Northcliffe and Schilling [90] or of Littmark and Ziegler [91]. It has also been shown that predictions of Lindhard-Scharff-Schiott theory (LSS) [92] underestimates ranges of slow heavy ions in matter. These discrepancies increase toward low energies up to 50% and more [93,94]. In this investigation the semiempirical method of Biersack [95] has been applied to get an estimate of recoil ranges in the target. According to this approach the equation for the nuclear stopping power is

$$S_n = \frac{4\pi\, a\, N\, A_i\, Z_i\, Z_t\, e^2}{A_i + A_t} \cdot \frac{\ln\varepsilon}{2\varepsilon(1 - \varepsilon^{-1.49})}, \qquad (2.18)$$

where $a = 0.8853 a_0 (Z_i^{1/2} + Z_t^{1/2})^{-2/3}$, a_0 is Bohr radius and N is the atomic density of the stopping medium. ε is the dimensionless energy converted from the recoil energy E_i,

$$\varepsilon = \frac{a\, A_t\, E_i}{Z_i\, Z_t\, e^2\, (A_i + A_t)} . \qquad (2.19)$$

The range (total path length of the recoil) is obtained by integrating over the inverse of the stopping power. Trajectories of heavy ions in this energy region are quite straight, corresponding well to the total path length of recoils. However, it has to be noticed that the evaporation of light particles (n,p,α) from the compound nucleus leaves the heavy recoils with some transverse momentum. This means the initial recoil beam has an angular spread, which will create changes in the final ranges. In order to obtain one curve for all the possible combinations of ions and stopping materials, the range R_t is replaced by the dimensionless range ρ,

$$\rho = \frac{4\pi\, N\, A_i\, A_t\, R_t\, a^2}{(A_i + A_t)^2} . \qquad (2.20)$$

In fig. 2-8 the calculated range as a function of the energy is shown graphically.

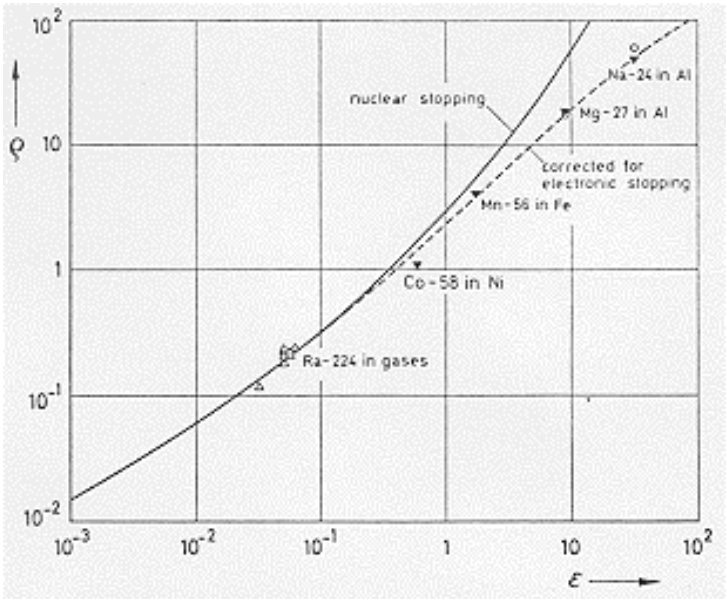

Fig. 2-8. The dimensionless range of recoils in matter as a function of dimensionless energy of recoils. The curve is based on theoretical calculations of Biersack. Some experimental data are also included. [95]

In each case the range can be determined by calculating the dimensionless energy ε, estimating graphically ρ from fig. 2-8 and calculating R_t from eq. 2.20. For higher energy recoils ($\varepsilon \approx> 0.3$) the electronic energy loss becomes more significant than the nuclear energy loss. This effect is included in the above curve. At higher energies the curve deviates ≈10 per cent of the values calculated from the LSS-theory.

In the present ion guide, only recoils with relatively low velocity can be thermalized in the gas phase. Lindhard and Scharff [96] have presented a formula for ranges of low velocity recoils ($V_i \approx < v_o$) in gases. Applying their formula to ion guide conditions, an equation giving average ranges in the helium buffer gas at pressure p is,

$$Rp = 8.23\ (A_i + 4)/Z_i\ (Z_i^{2/3} + 2.52)^{1/2}\ E_i/A_i\ . \qquad (2.21)$$

The numerical coefficient corresponds to the units of mbar-cm for Rp and keV/u for E_i/A_i. Figure 2-9 presents the dependence of Rp on the recoil energy for ions with Z_i= 20, 50 and 80. It has to be noted that the gaussian-shape distributions of recoil ranges in helium are rather wide at the pressure region used. For example, Bryde et al. have measured the average range of ^{66}Ga recoil ions of 18keV/u to be ≈10 cm and the range distribution as wide as ≈8 cm (FWMH) at the pressure of ≈130 mbar [97]. This means that about half the recoils are stopped within a distance corresponding to the average range R.

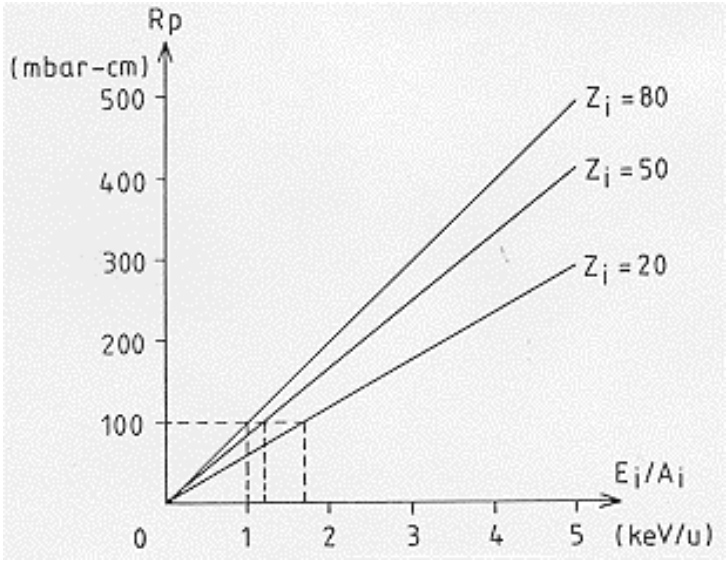

Fig. 2-9. Average range times pressure for low-energy recoils Z_i= 20, 50 and 80 in helium as a function of recoil energy. The curves are based on eq. 2.21. Dashed lines indicate the stopping conditions of recoils in the present ion guide.

Figure 2-10 presents schematically a thick target arrangement in the target chamber of the ion guide. In this connection "thick" means that the thickness of the solid target is more than the maximum range of recoils in that material.

The stopping efficiency of the ion guide can be defined as

$$\varepsilon_{stop} \approx \frac{xp_{tc}}{Rp} = \frac{d}{R_t} = \frac{Y_d}{Y}, \qquad (2.22)$$

where Y corresponding to R_t, is the total number of recoils leaving the target. Y_d is the number of thermalized recoils, corrresponding to the number of recoils emitted from the thickness d. In this consideration the effect of angular distribution of recoils is excluded. For low energy recoils the factors Rp and R_t can be calculated from eq:s 2.21 and 2.20. For practical purposes thermalization is complete if the condition $\varepsilon_{stop} \geq 1$ is fulfilled.

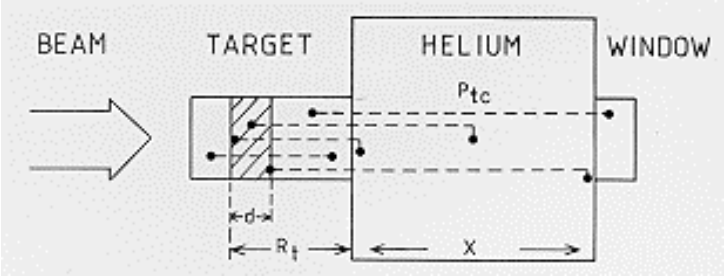

Fig. 2-10. A schematic drawing of target and buffer gas arrangements in the target chamber of the ion guide. The black points represent recoils from nuclear reactions. Their path in the target and in the helium buffer gas is shown by broken lines. The symbols have the following meaning: d is the thickness for recoils stopped in the gas phase; R_t is the effective target thickness; x is the stopping distance and p_{tc} the helium pressure in the target chamber.

Because the product xp_{tc} (=constant) determines the maximum kinetic energy of the recoils thermalized in helium, it turns out that nearly constant number of atoms (N_d) are contained in the volume corresponding to the thickness d in any target with Z_t>10, and in any type of reaction. If the beam energy is higher, it follows that R_t increases (ε_{stop} decreases), but d has still the same value. Only the position of the width d goes deeper inside the target. The number of atoms within d is calculated from the equation

$$N_d \approx S_t\, N_o\, \varepsilon_{stop}\, R_t / A_t$$

$$= \frac{S_t\, N_o\, R_t}{Rp\, A_t}\, xp_{tc}\,, \qquad (2.23)$$

where S_t is the cross-sectional area of the target (cm^2) and N_o is Avogadro's constant. R_t, the range in the target is here given in g/cm^2. For the ion guide with xp_{tc}= 100 mbar-cm and S_t= 1 cm^2, N_d is of the order of (2-5)x10^{17} atoms. In this numerical estimation the initial recoil energy is determined on the basis of conservation of linear momentum excluding the effect of breakup of the assumed compound nucleus. For example, with the projectile beam intensity of 1 pμA, the number of recoils per unit time and unit reaction cross-section thermalized in helium should then be

$$Y_d / \sigma_r \approx 1000\text{-}3000 \text{ atoms/s-mbarn} \quad ,$$

independent of the reaction.

2.3. *Motion of thermalized recoil ions in helium*

2.3.1. Diffusion and mobility of ions

Immediately after their thermalization in high pressure helium recoil ions are transported out of the target chamber by the flowing gas. During transportation ions diffuse randomly and losses of ions take place on collisions with the chamber walls. In principle, the amount of losses can be reduced by controlling the motion of ions by external electric fields. An equation [78] which defines the flux of positive ions in a steady state gas is

$$\vec{\Gamma} = - D \vec{\nabla} n_i + \mu n_i \vec{F} , \qquad (2.24)$$

where D is the diffusion coefficient, n_i is the number density of ions, μ is the mobility and F is the external electric field.

The diffusion coefficient is defined as

$$D = \frac{kT}{m\nu} , \qquad (2.25)$$

where k is Boltzmann constant, T is temperature of the gas, m is the reduced mass of the system composed of a buffer gas atom and an ion, and ν is the collision frequency.

The mobility of the +1-charged ion is determined by the formula

$$\mu = \frac{e}{m\nu} . \qquad (2.26)$$

The drift velocity of ions under an electric field is then,

$$V_d = \mu F . \qquad (2.27)$$

Both transport coefficients can be connected to each other by Einstein relation

$$\mu = \frac{eD}{kT} , \qquad (2.28)$$

which at room temperature is approximately equal to $\mu \approx 40D$, with the units $[\mu] = cm^2/Vs$ and $[D] = cm^2/s$.

The mobility is connected to the reduced mobility μ_o through the relation

$$\mu = \frac{p_o}{p} \frac{T}{T_o} \mu_o , \qquad (2.29)$$

where $p_o = 1000$ mbar, p is the gas pressure, $T_o = 273$ K and T is the gas temperature. A value which is accurate enough for practical purposes for reduced mobility of ions (with $Z_i > 2$) in helium [98], is

$$\mu_o \approx 20 \text{ cm}^2/\text{Vs} .$$

A reasonable estimate for the diffusion coefficient of any ion ($A_i \approx > 10$) in room temperature helium can be calculated from the equation

$$D \approx \frac{500}{p} , \qquad (2.30)$$

where the units are cm^2/s for D and mbar for p.

The three-dimensional density distribution,

$$n_i/N_i = [(4\pi Dt)^{3/2} \exp(r^2/4Dt)]^{-1} , \qquad (2.31)$$

gives the relative number of ions diffused over distance r from a point source in time t [99]. The total number of ions at the moment t=0 is N_i. Typically diffusion distributions are wide. The curves in fig. 2-11 represent calculated diffusion distributions related to various ion guide parameters. In each case the point source of ions is assumed to be located in the center of the target chamber.

The probability for the loss of ions to the chamber walls as a function of time is deduced from the relative area of the diffusion distribution $S_D(t)/S_D(\infty)$. The area or a part of it is found from the integral

$$S_D = \int_{t_1}^{t_2} n_i/N_i \, dt = (4\pi Dr)^{-1} [\, erf(z_1) - erf(z_2) \,] \, , \quad (2.32)$$

where the variables of the error functions are $z_1 = r\,(4Dt_1)^{-1/2}$ and $z_2 = r\,(4Dt_2)^{-1/2}$ [100].

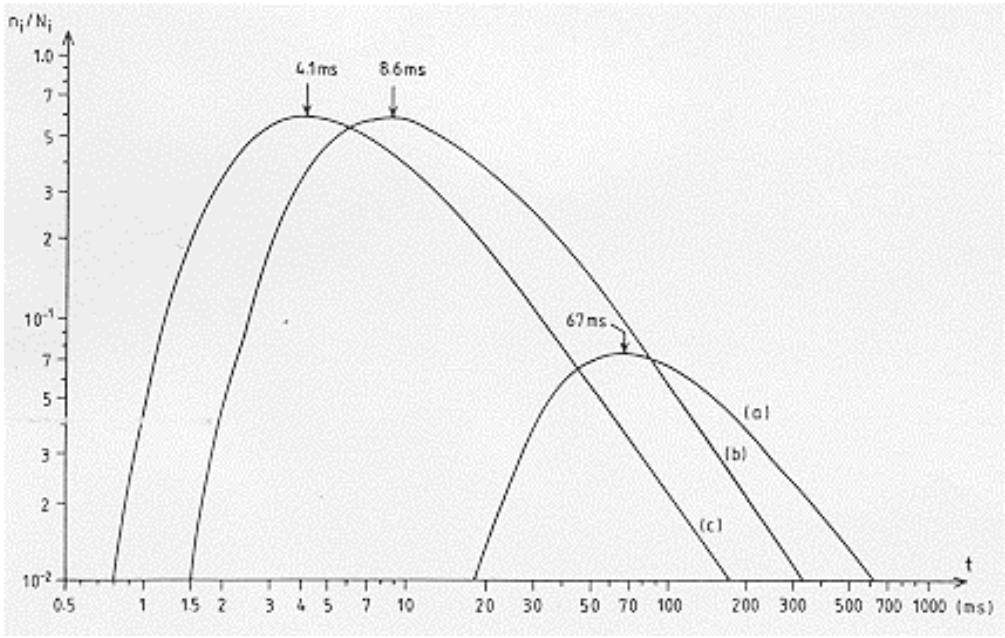

Fig. 2-11. Three-dimensional density distributions of recoil ions diffusing in the target chamber of the ion guide as a function of time.

(a) D= 2.5 cm^2/s, r= 1.0 cm (off-line),
(b) D= 5.0 cm^2/s, r= 0.5 cm (on-line),
(c) D_a= 10 cm^2/s, r= 0.5 cm (on-line).

The curves are based on eq. 2.31. The values of the diffusion coefficients correspond to experimental pressure conditions and the distances of the shortest path to the chamber wall (refer to table 3-3).

The average displacement of ions in time t is

$$\bar{r} = (16\,Dt/\pi)^{1/2} \quad . \qquad (2.33)$$

In an infinitely long cylinder of radius r_o the most probable diffusion time of an ion to the chamber wall is [99],

$$\bar{\tau}_D = (r_o/2.405)^2 / D. \qquad (2.34)$$

The average total kinetic energy of an ion drifting through helium under electric field F can be presented in the form [101],

$$\bar{E}_i = 5.22\text{x}10^{-13}\,(A_i + 4)\,(\mu F)^2 + 1.29\text{x}10^{-4}\,T\,, \qquad (2.35)$$

where the numerical coefficients correspond to the units eV, u, cm^2/s, V/cm and K, respectively.

Applying the above equation to typical conditions in off-line operation with radioactive recoil ions, where A_i= 215 u, the pressure is 100 mbar, F< 10 V/cm and T≈ 293 K, it can be found that the thermal energy dominates the motion of ions: the kinetic energy due to the drift velocity is ≈<0.5 meV, while the thermal energy is kT≈ 25 meV.

As long as external electric fields are weak, i.e. F/p≈< 1.5 V/cm-mbar, the above equations are valid. With higher values of the parameter F/p the mobilities and diffusion coefficients are no longer constant [84,99].

The use of a magnetic field B as a means of controlled ion transportation in the gas does not seem applicable. The basic idea is to reduce the perpendicular diffusion rate so that ions will follow the magnetic field lines. A condition for the successful working of this phenomenon is [78],

$$(\mu B)^2 \;\gg\; 1. \qquad (2.36)$$

This relation reveals that magnetic fields of practical strength are useful only in dilute gases (≈<0.1 mbar). This view conforms with experimental results, which showed no effect in transport of recoil ions when the parameters B≈ 1 kG and p_{tc}= 100 mbar were applied.

2.3.2. Motion of ions in a weak plasma

In on-line conditions a weak plasma is created by the accelerator beam in helium buffer gas. Because of their light mass, electrons are much more mobile than ions in the gas. Electron mobilities are two to three orders higher than ion mobilities [80]. However, the plasma tends to keep its neutrality, i.e., $n_e=n_i=n$: If electrons in the plasma are displaced from a uniform background of ions, electric fields will be built up in such a direction as to restore the neutrality of the plasma by pulling electrons back to their original positions. This is reflected in the motion of ions and electrons in the plasma so that the rates of diffusion of ions and electrons are equal, $\Gamma_i = \Gamma_e$.

$$\Gamma = - D_i \nabla n + \mu_i n F = - D_e \nabla n - \mu_e n F . \qquad (2.37)$$

The common flux can be presented as

$$\Gamma = D_a \nabla n , \qquad (2.38)$$

where the new coefficient, the ambipolar diffusion coefficient is

$$D_a = \frac{\mu_i D_e + \mu_e D_i}{\mu_i + \mu_e} . \qquad (2.39)$$

In plasma, the diffusion of two species is thus controlled by the effect of the ambipolar electric field equalizing the diffusion rates. Usually, $\mu_e \gg \mu_i$ and the ambipolar diffusion coefficient has the form

$$D_a \approx D_i (1 + T_e/T_i) . \qquad (2.40)$$

In equilibrium conditions with $T_e \approx T_i \approx T$, the ambipolar diffusion is controlled by the ions,

$$D_a \approx 2D_i \, . \qquad (2.41)$$

The use of an external electric field through a plasma for controlling the motion of ions, is restricted by Debye length, which is defined as

$$\lambda_D = [\, kT_e / (4\pi n_e e^2) \,]^{1/2} \, . \qquad (2.42)$$

A practical form of eq. 2.42 is

$$\lambda_D = 740 \, (kT_e/n_e)^{1/2} \, , \qquad (2.43)$$

where the units are cm for λ_D, eV for kT_e and cm^{-3} for n_e. Debye length is related to another fundamental characteristic of the behaviour of plasma, which is its ability to shield off electric potentials that are applied to it. The decrease of external potential S in the plasma follows the formula

$$S = S_o \, \exp (-x/\lambda_D) \, , \qquad (2.44)$$

where S is the potential at the distance x=0 from the electrode [78].

The information given in this chapter is needed in the calculation of the ion guide parameters and also in the evaluation of the experimental results.

3. EXPERIMENTAL TEHCNIQUES AND RESULTS

3.1. *Construction of the ion guide*

3.1.1. Principle of operation

The operation of the ion guide is based on a helium-jet technique [12-19] modified to provide radioactive recoils as +1-charged, atomic ions.

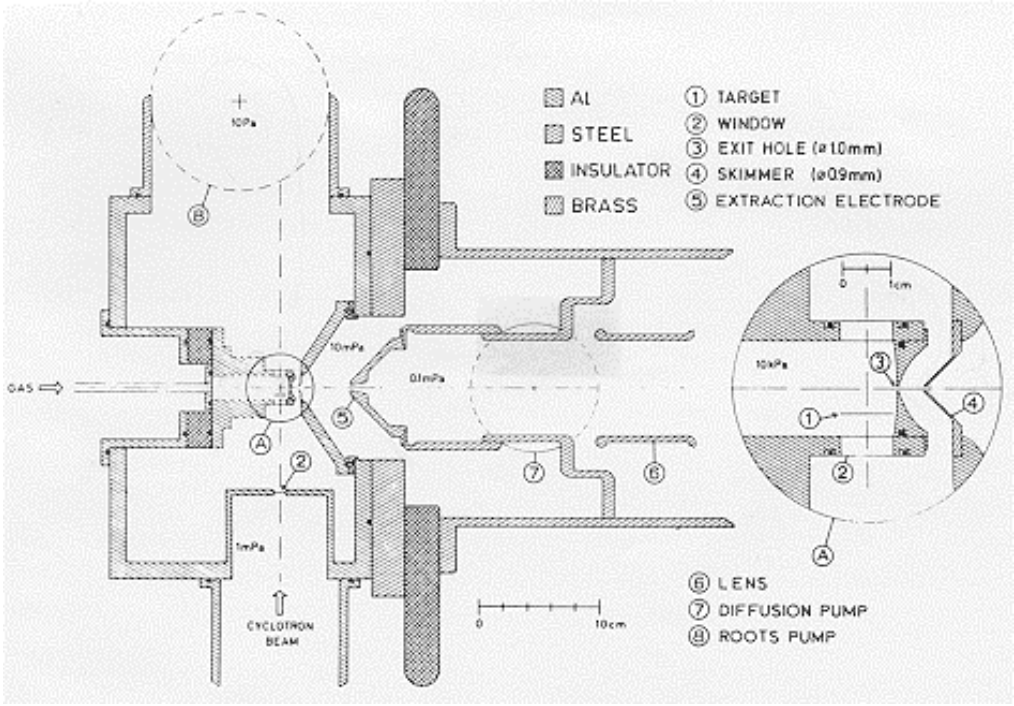

Fig. 3-1. Layout of the ion guide system and its connection to the extraction chamber of the isotope separator.

The construction of the ion guide is shown in fig. 3-1. The target or a radioactive source is placed in the helium-filled, cylindrical chamber. Commercial helium was used in experiments and impurity molecules in the gas, reported by the distributor, were Ne< 10 ppm, N_2< 10 ppm, O_2< 5 ppm and H_2O< 10 ppm. In addition of these, other sources for impurity molecules are leakages in gas tubes and valves, water vapours on the

walls of the target chamber and evaporation of seal materials. The resulting total amount of impurities within the helium is estimated to be of the order of 100 ppm.

A large proportion of the recoils remain charged when they are thermalized in collisions with helium atoms and impurity molecules. The recoils are swept along with gas through an exit hole into an adjacent vacuum chamber. The exit hole of the target chamber is placed in the middle axis of the accelerating section of the separator. The target chamber and the extraction electrode of the separator are separated by a skimmer hole. Electric fields between the exit, skimmer and the extraction electrode form an electrostatic lens system. In this arrangement the skimmer acts as a grid which guides positive ions into the separator for further acceleration. On the other hand, the skimmer has to prevent neutral helium from flowing into the extraction volume of the separator. Removed helium is pumped out of the vacuum chamber by means of a high-speed Roots blower. This arrangement replaces a conventional ion source.

The isotope separator is of a Scandinavian type, having an analyzing magnet with the 55°-deflection and 1.5 m radius of curvature. The maximum accelerating voltage is 50 kV. Improved stability of the separator and an automatic mass-selection are realized by a microcomputer based monitoring and handling system. The magnetometer has the precision of 0.01 G, in the range from 0.95 kG to the maximum field strength of the magnet, 4.5 kG. Adjustment and regulation of the field are carried out by the stepping motor control of the power supply. The ion beam transportation through the separator is performed by conventional beam handling methods.

3.1.2. Constructional parameters

The constructional parameters of the ion guide with their symbols and typical values used in on-line experiments are gathered in table 3-1.

Parts and parameters	Symbol	Typical value
Target chamber:		
volume	V_{tc}	≈1 cm^3
radius	r_{tc}	0.5 cm
stopping distance	x	≈1 cm
diameter of exit hole	ϕ_e	1.2 mm
Vacuum chamber:		
dimensions		20x20x30 cm^3
diameter of skimmer hole	ϕ_s	1.5 mm
cone height of skimmer	h_s	2-6 mm
exit-skimmer distance	x_{es}	6-13 mm
exit-skimmer voltage	V_{es}	-0.5 - -1 kV
Extraction chamber:		
hole diameter in extractor	ϕ_{ext}	4.2 mm
skimmer-extractor distance	x_{ext}	2-4 cm

Table 3-1. Constructional parameters of the ion guide and the extraction chamber of the separator.

In the following chapters these parameters are valid. Where a parameter differs from the above value, it is mentioned and a new value is given.

3.1.3. Pumping system and related flow parameters

Two technical parameters play a central role in determining the efficiency of the ion guide: the evacuation time of the target chamber and the helium pressure inside it. A short evacuation time and high pressure are realized by using a high speed pumping system.

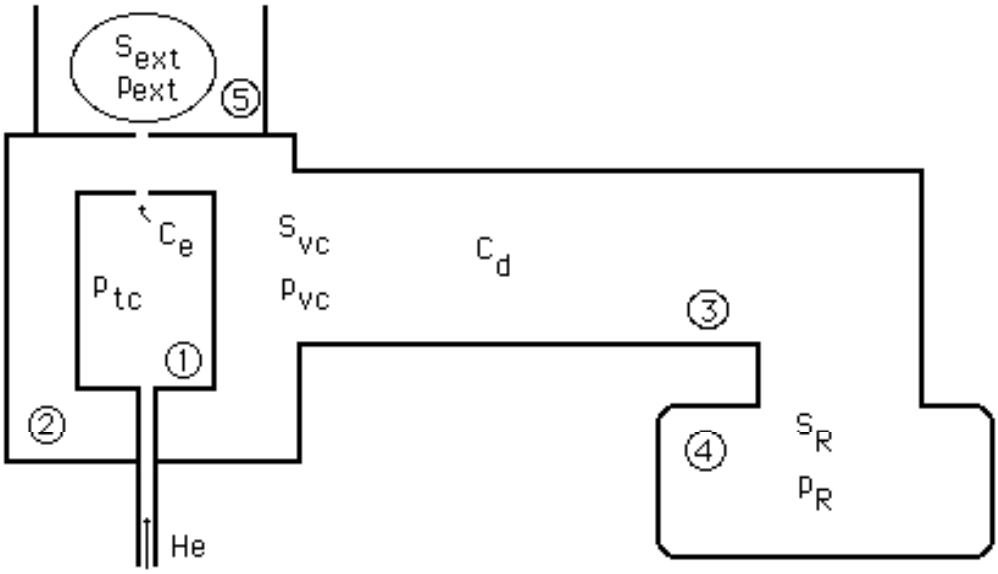

Fig. 3-2. Schematic drawing of the pumping arrangement of the ion guide and the extraction chamber of the separator.
1. Target chamber, 2. vacuum chamber, 3. Roots pumping line,
4. Roots blower, 5. extraction chamber of the separator.
See values of the parameters in table 3-2.

In fig. 3-2 the pumping arrangement of the ion guide is shown schematically. In this arrangement the target chamber, the vacuum chamber, the pumping line and the Roots blower are connected in series. This means that the gas throughputs of those sections are equal,

$$Q_{tc} = Q_{vc} = Q_d = Q_R \equiv Q . \qquad (3.1)$$

Some gas flows into the extraction volume of the separator. However, the amount of that flow is only about one per mille of the total throughput.

The throughput or mass flow rate Q (at constant temperature) is defined by the equations,

$$Q = C\,\Delta p = S\,p , \qquad (3.2)$$

where C is the conductance of the pumping channel, Δp is the pressure difference between two adjacent chambers and S is the pumping speed at pressure p.

The pumping speed in the target chamber which is connected in series with the vacuum chamber by an exit hole, can be calculated from the equation

$$1/S_{tc} = 1/S_{vc} + 1/C_e \ . \qquad (3.3)$$

Due to the high helium pressure the gas flow through the target chamber and the exit hole is viscous. Based on the laws of adiabatic expansion and on eq. 3.2, the conductance of a small exit hole can be determined from the equation [102],

$$C_e = \frac{Q}{p_{tc} - p_{vc}} \qquad (3.4)$$

$$= \frac{A_e p_{tc}}{p_{tc} - p_{vc}} (p_{vc}/p_{tc})^{1/\gamma} \{ 2\gamma /(\gamma-1) (R_0 T/A) [1- (p_{vc}/p_{tc})^{(\gamma -1)/\gamma}]\}^{1/2},$$

where p_{tc} = pressure in target chamber,
p_{vc} = pressure in vacuum chamber,
$A_e = \pi\phi_e^2/4$ = cross-sectional area of exit hole,
$\gamma = c_p/c_v$ = ratio of specific heats at constant pressure and volume = 1.659 for helium,
R_o = gas constant,
T = gas temperature
and A = atomic mass of buffer gas.

The solution of the above equation in typical operating conditions gives a simple relation between the conductance and the diameter of the exit hole,

$$C_e \approx 0.45 \ \phi_e^2 \ , \qquad (3.5)$$

where the units are l/s for C_e and mm for ϕ_e. In practice the conductance of the exit hole alone determines the pumping speed of the target chamber, because the value of C_e is small compared to that of S_{vc}. The evacuation time of the target chamber of volume V_{tc} or the residence time of an ion in the volume V_{tc} can now be written as

$$t_{tc} = V_{tc}/S_{tc} \approx V_{tc}/C_e \ . \qquad (3.6)$$

Throughput of helium:	Q	$\approx$	65 mbar l/s
	Q_{ext}	$\approx<$	0.1 mbar l/s
Pressures:	p_{tc}	=	100 mbar
	p_{vc}	=	0.24 mbar
	($\approx>10^{-4}$ mbar without helium flow)		
	p_R	=	0.12 mbar
	p_{ext}	$\approx<$	2×10^{-4} mbar (above the baffle)
Conductances and pumping speeds:			
	C_e	$\approx$	0.65 l/s
	S_{tc}	$\approx$	0.65 l/s
	S_{vc}	$\approx$	275 l/s
	C_d	$\approx$	550 l/s
	S_R	=	555 l/s (2000 m^3/h)
	S_{ext}	$\approx$	650 l/s (with the baffle)

Table 3-2. Pumping parameters and related flow parameters of the ion guide equipped with the exit hole of ϕ_e= 1.2 mm, and with the 1.5 mm diameter skimmer at x_{es}= 8 mm. The symbols refer to fig. 3-2.

The average transport velocity of a recoil ion in the gas stream is obtained from the equation,

$$v_f = \frac{Q}{p_{tc}\ A_{tc}} \ . \qquad (3.7)$$

Here A_{tc} is the cross-sectional area of the target chamber and the throughput is exceptionally expressed in units mbar cm^3/s. It is also assumed that the collision frequency, $>10^8$ s^{-1}, is high enough to give a recoil velocity which equals that of the helium flow.

Table 3-2 presents the parameters related to the pumping system of the ion guide and the extraction chamber of the separator. The above throughput and pressure values are used in on-line operation.

The Roots blower is connected to the vacuum chamber by 3.5 meter long pumping line having one 90° curve. The effective diameter of the line is 15 cm. Originally the pumping speed of the diffusion pump in the extraction chamber is 1300 l/s. In practice the baffle reduces its capacity to half of that value.

Although the helium flow into the extraction chamber is only about one per mille compared to the total flow, it seriously limits the efficient operation of the present IGISOL. In that chamber the vacuum of $2x10^{-4}$ mbar has turned out to be the maximum usable value. Higher pressure results in poor resolving power of the separator and unstable operating performance.

3.1.4. Calculated values of the transport parameters

As mentioned earlier, the main reasons for losses of recoil ions are believed to be their diffusion to the chamber walls during the transportation. In on-line conditions extra losses are due to long recoil ranges. As long as recoils are stopped in helium, they seem to have a good probability of surviving as ions during the transportation out of the target chamber. Both the diffusion rate and the range of the recoil can be reduced simply by increasing the helium pressure in the chamber. In addition to
these parameters, the evacuation time of the target chamber should be shorter than the average diffusion time of ions to the chamber walls. For the present ion guide this is demonstrated in fig. 3-3, where the difference between times of evacuation and average diffusion, and the

consequence of that difference are presented. The growth of the relative area of the diffusion distribution as a function of time is calculated for two values of D, 5 and 10 cm^2/s. The curves are based on eq. 2-32 with r = 0.5 cm (the average distance to the target chamber wall). The reference area S_D corresponds to the total area of the distributions (b) and (c), presented in fig. 2-11.

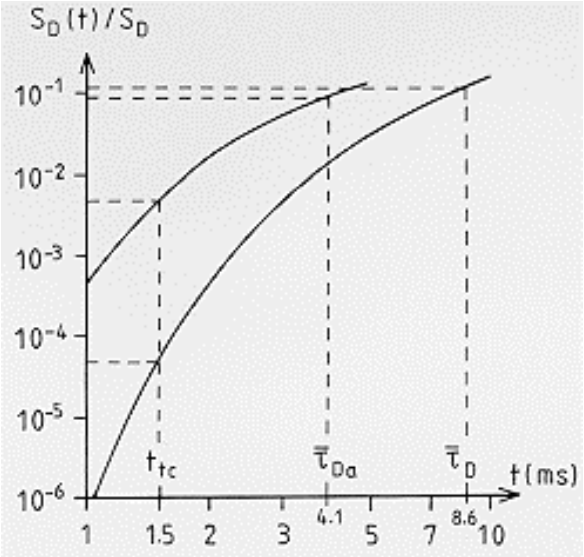

Fig. 3-3. Growths of relative areas of diffusion distributions as a function of time. The curves correspond to the distributions (b) and (c) in fig. 2-11. S_D corresponds to the total area in each case.

From the dashed lines (at τ_D and τ_{Da}) it can be seen that about 10 per cent of the ions are lost to the chamber walls in a period of time which equals the average diffusion time of an ion. A short enough evacuation time (t_{tc}), however, ensures that the ions can be transported effectively out of the chamber before they are lost to the walls. It has to be noted that the above case is an ideal one, where ions diffuse a fixed distance from the point source. In the real system the ions are initially spread all over the target chamber and half of them can be assumed to have a path shorter than the average distance to the chamber wall. That makes short evacuation time even more important.

Table 3-3 presents average values for calculated transport parameters of the ion guide in three different cases. The calculations are

based on the equations presented in chapters 2.3 and 3.1.3, and on such experimental parameters which gave the best yield of recoil ions in each case.

Dimensions of target chamber:

Volume V_{tc} (cm^3)	Radius r_{tc} (cm)	Diameter of exit ϕ_e (mm)	Transport distance y (cm)
75	2.0	0.35	2.0
20	1.0	0.65	2.0
1	0.5	1.2	0.5

Flow parameters:

Pressure p_{tc} (mbar)	Exit conductance C_e (l/s)	Throughput Q (mbar l/s)	Evacuation time t_{tc} (ms)
400	0.055	22	1360
200	0.19	38	105
100	0.65	65	1.5

Transport parameters:

Diffusion coefficient D (cm^2/s)	Mobility μ (cm^2/Vs)	Electric field F (V/cm)	Flow time t_f (ms)	Diffusion time τ_D (ms)	Drift time t_d (ms)
1.25	54	1.0	450	550	40
2.5	107	0.27	33	70	67
5 ; 10			0.7	4.1 ; 8.6	

Table 3-3. Calculated flow and transport parameters related to the different target chambers of the ion guide. The first two rows in each section describe the properties of the chambers used with the radioactive source. The third rows describe the chamber used in on-line experiments.

In off-line conditions an electric field between the recoil source and the chamber wall increased the yield of ions, contrary to the results measured in on-line experiments. In the latter case the apparent reason is the plasma which disturbs electric fields (eq. 2.44).

The value of the diffusion coefficient in on-line conditions is difficult to know exactly. Therefore two values are reported, D= 5 cm^2/s without the projectile beam, and D_a= 10 cm^2/s, an estimated ambipolar diffusion coefficient in the helium plasma [81,103].

In addition to transport through the target chamber, ions are further accelerated at a relatively high gas pressure between the exit and skimmer
holes using a strong electric field, ≈ 0.4-3.7 kV/cm. The pressure gradient in that space is large. The mobility of ions may change very rapidly and may achieve values which are dependent on the electric field. Altogether the situation between the exit and the skimmer becomes so complex that the estimate of transport parameters there is very difficult. The effect of the gas between the exit and the skimmer on the kinetic energy of ions is, however, treated in chapter 3.3.3 on the basis of experimental results.

3.2. *Off-line experiments*

3.2.1. Spark discharge ion source for off-line development

3.2.1.1. Construction

The simpliest way to get ions for the development purposes of the ion guide separator is to use a discharge between electrodes in the target chamber. Fig. 3-4 shows schematically the spark discharge ion source inside the usual target chamber. The electrodes are made of stainless steel and the tips of the electrodes are sharp.

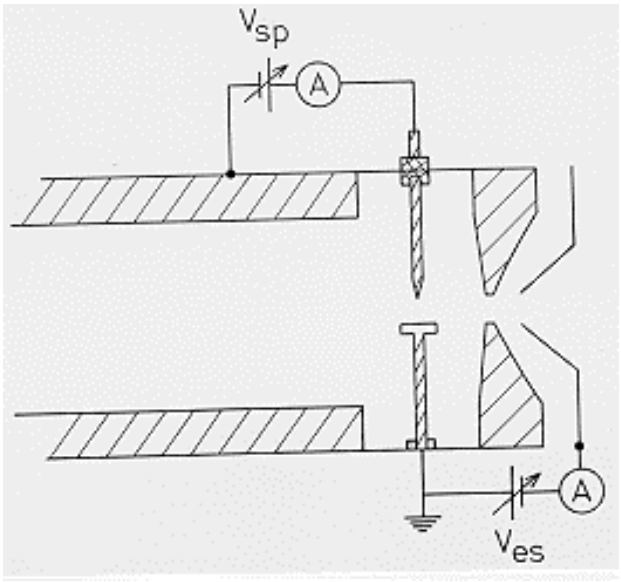

Fig. 3-4. Spark discharge ion source in the target chamber of the ion guide. V_{sp} = spark voltage, V_{es} = skimmer voltage, A = current meter.

For stable operation optimum distances between the two electrodes and between the electrodes and the exit hole were found to be ≈1.4 mm and ≈3 mm, respectively. Discharge voltage is dependent on the distance between the electrodes and on the gas pressure [104]. A spark between two separate electrodes was found more stable than that between one electrode and the wall surrounding the exit hole. Helium flow and the

other ion guide parameters were about the same as in typical on-line conditions.

3.2.1.2. Some experimental results

The total positive current emerging out of the target chamber was measured at the skimmer position. The skimmer hole was closed which ensured that all of the ion current was collected. The current of positive ions reached saturation after the skimmer voltage had the value of ≈ -15V (fig. 3-5).

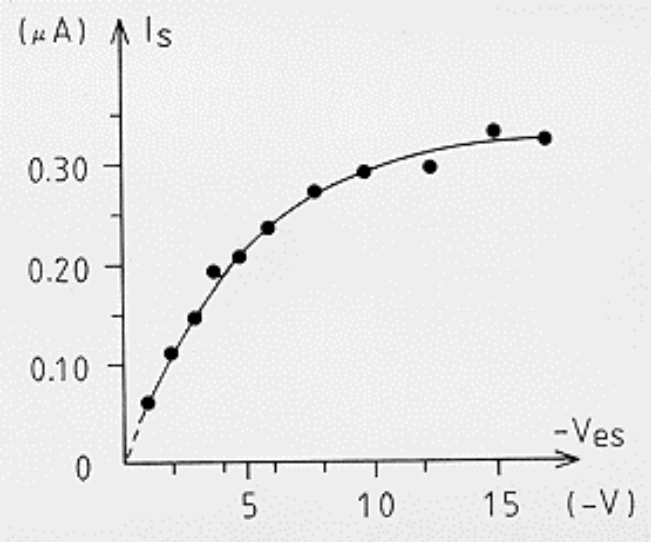

Fig. 3-5. The positive ion current on the closed skimmer plate as a function of skimmer voltage.

The following ion guide parameters: V_{tc}≈ 20 cm^3, p_{tc}= 120 mbar, ϕ_e= 1.0 mm, x_{es}= 7 mm, V_{sp}= 240 V and the spark current of 2.5 μA produced the saturated positive ion current of I_s= 0.32 μA. This resulted in a transport efficiency of ≈13%. Correspondingly, in the same conditions the negative current due to electrons and negative ions was I_s= -0.062 μA.

The positive ion current was also measured after the high voltage acceleration in front of the analyzing magnet of the separator. The

diameter of the collector plate was 40 mm and the measured current 0.2 μA, which gave a transmission efficiency of 60% through the skimmer (ϕ_s= 1.5 mm, h_s= 7.0 mm, V_{es}= -150 V).

In the next step the ion current was mass separated and measured by a picoammeter connected to a Faraday-cup with the slit of 15 mm. All masses, except those at atomic masses of 6, 7, 9, 10, 11, 22, 23 and 47 were present in the spectrum below the heaviest detected mass 52. Table 3-4 presents the currents of the most intensive ion beams and probable identities of the ions.

A_i (u)	I_A (nA)	Ion
4	0.35	He^+
14	1.9	N^+
16	7.4	O^+
17	3.0	NH_3^+, OH^+
18	0.92	H_2O^+
19	0.42	$H^+(H_2O)$
28	0.98	N_2^+
32	0.085	O_2^+

Table 3-4. Mass separated currents of stable ions and their probable identities. The spark current was 2.4 μA and the integrated current ≈0.015μA.

An integration of the mass separated currents yielded an overall efficiency of ≈0.6%. In that measurement the ion beam of the separator was focused at the mass A_i= 16 and using the skimmer voltage of -600 V. It was found that the currents of different molecular ions behave differently as functions of the skimmer voltage. Thus the overall efficiency determined this way provides a rough estimate only. For example, the best yield of H_2O^+ ions were reached with the skimmer voltage of -150 V. With higher values of V_{es} the H_2O^+ current decreased rapidly, indicating a dissociation of H_2O molecules [88] between the exit and the skimmer. At the same time the current of O^+ increased until the skimmer voltage reached -600 V, after which it was saturated (fig. 3-6).

It must be noted that there is no remarkable difference in the mass spectrum of stable ions initiated by the spark discharge ion source or produced by the projectile beam in on-line conditions (ch. 3.3.3). Also

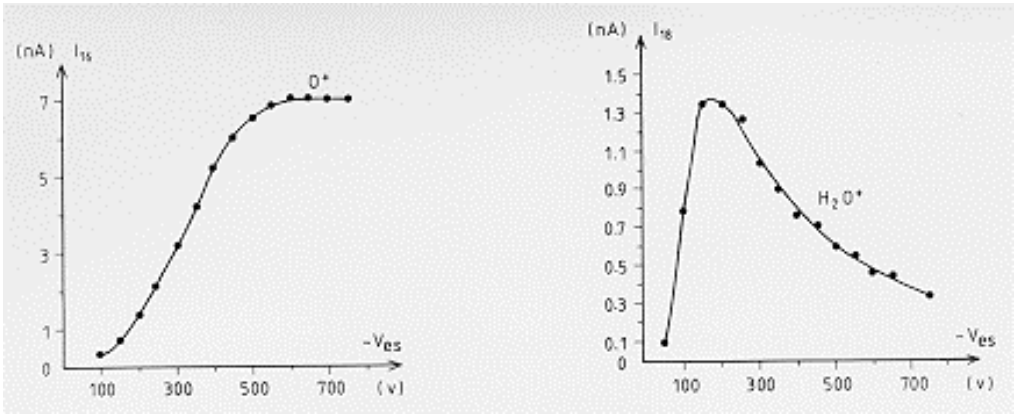

Fig. 3-6. Mass separated currents of stable ions O^+ and H_2O^+ as a function of the skimmer voltage. For O^+ the spark current was 2.35 μA and the aperture of the Faraday-cup was 15 mm, while for H_2O^+ they were 1μA and 3 mm.

ionization due to α-particles from the ^{227}Ac source produces the same kind of spectrum, although the currents are smaller because the α-source used was weak.

3.2.2. Use of an α-active ^{227}Ac recoil source for development of the ion guide

The ion guide method was basically developed by using α–recoils from the ^{227}Ac source. The use of the radioactive source has been found very applicable also in a further development of the method. The only remarkable differences compared to on-line conditions are shorter ranges of recoils, and a lower degree of ionization of the buffer gas. Thus, the use of the radioactive source can be considered more or less as a simulation for on-line use. A great advantage is that the yield of radioactivities from the source is constant and not sensitive to different

parameters as is the current of stable molecular ions from the spark discharge ion source or as is the yield of radioactive recoils induced by the accelerator beam.

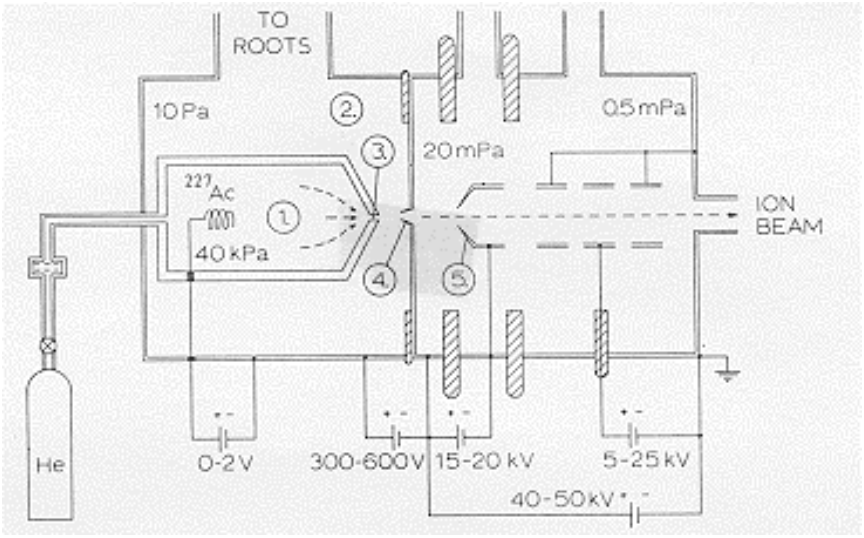

Fig. 3-7. Ion guide connected to the accelerating section of the isotope separator [22]. The geometrical dimensions are not drawn to scale.
(1) Recoil chamber, (2) vacuum chamber, (3) capillary or exit hole,
(4) skimmer, (5) extraction electrode.

Figure 3-7 presents schematically the connection of the ion guide to the accelerating section of the isotope separator. The radioactive source is placed in a helium-filled recoil chamber which is cylindrical, rounded at one end, and 75 cm^3 or 20 cm^3 in volume. Recoils are emitted into the gas both directly from the wire source and via disintegrations in the helium buffer gas.

3.2.2.1. Radioactive ^{227}Ac recoil source and detection facility

The actinium isotope 227 was electrolytically deposited on the surface of a spiral-shaped tantalum wire (diameter ≈ 0.5 mm). Figure 3-8 presents the decay scheme of the actinium series from the isotope ^{227}Ac to the stable ^{207}Pb.

The actinium decays to lead via five alpha and three ß⁻-decays. The long lived isotopes ^{227}Ac, ^{227}Th and ^{223}Ra ensure a constant production rate of ^{219}Rn, the daughter nuclei of radium. The activity of radium was measured to be ≈7.5x10^5 Bq (≈20 μCi).

It should be noted that practically all of the recoil particles emitted from the source and transported through the capillary or the exit hole can be collected onto a catcher surface if such a surface is placed in front of the exit in the vacuum chamber. Radon being an inert gas is an exception; it does not adhere to the surface at room temperature.

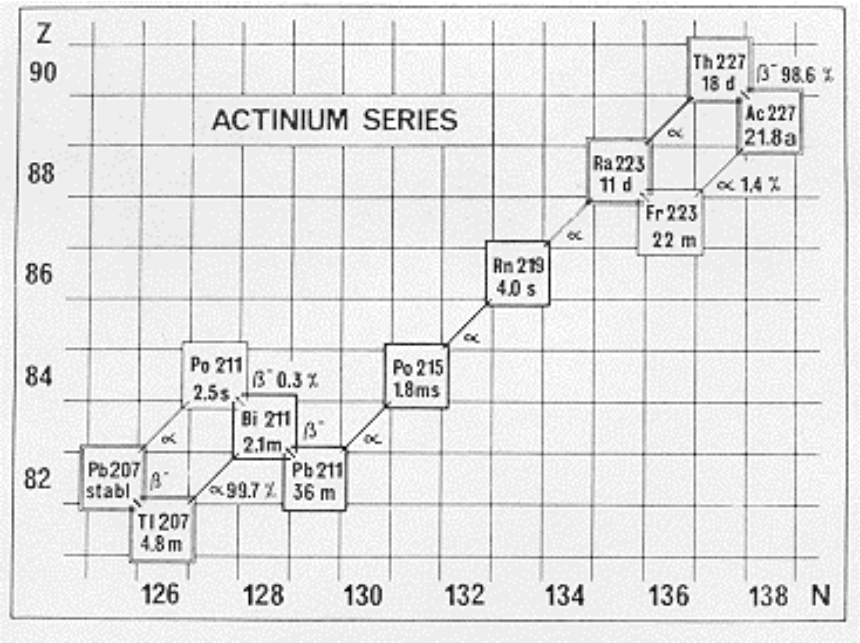

Fig. 3-8. The latter part of the decay chain of the actinium series. [23]

Investigations before connection of the ion guide to the separator were made by using a recoil chamber having a large volume (V_{tc}≈ 75 cm^3). The flow rate of helium was regulated so that a large fraction of the disintegrations of radon took place in this chamber. The recoils collected on the mylar tape were mainly the isotope ^{211}Pb. The α–activity of ^{211}Bi (E_α= 6.28 and 6.62 MeV) on the tape was then observed with a Si(Au)- surface barrier detector, 100 mm^2 in area and 100 μm thick. A tape transport apparatus was used for collecting samples and moving them to the front of the detector. The mylar tape

was coated with aluminium on one side and was isolated to withstand electric potential when desirable. It could be used in front of the recoil chamber or it could be mounted in the collection chamber of the isotope separator. This provided equal experimental conditions for comparing mass separated samples with those collected at the skimmer position. For instant direct detection of the mass separated, short-lived (1.8 ms) ^{215}Po, a 300 mm^2 annular surface barrier detector with the hole of 4 mm was used.

3.2.2.2. Experiments without the isotope separator

The purpose of the following experiments, primarily, was to find out if there were ionized recoils among the activity thermalized in helium. Secondly it was investigated if it was possible to transport the recoils out of the recoil chamber as ions. The results of these measurements showed the solution for the connection of the ion guide to the isotope separator.

Figure 3-9 presents a drawing of the 75 cm^3 recoil chamber and the capillary-skimmer arrangement used in these experiments.

The curve in fig. 3-10 shows the α–activity deposited onto the transport or collector tape at various distances (x_c) from the capillary exit. The flow rate of the helium was optimized to give the highest yield of ^{211}Pb. The yield remained relatively constant over the distances $4 \approx< x_c \approx< 8$ mm, between the capillary and the collector tape. In this basic experiment the flow and transport parameters were as they appear in the first rows in table 3-3. In all measurements the collection time of the activity was 10 min and the measuring time was 8 min. The time interval between collection and start of the activity measurement was 2 min. Also the values of the ion guide parameters were constant in the

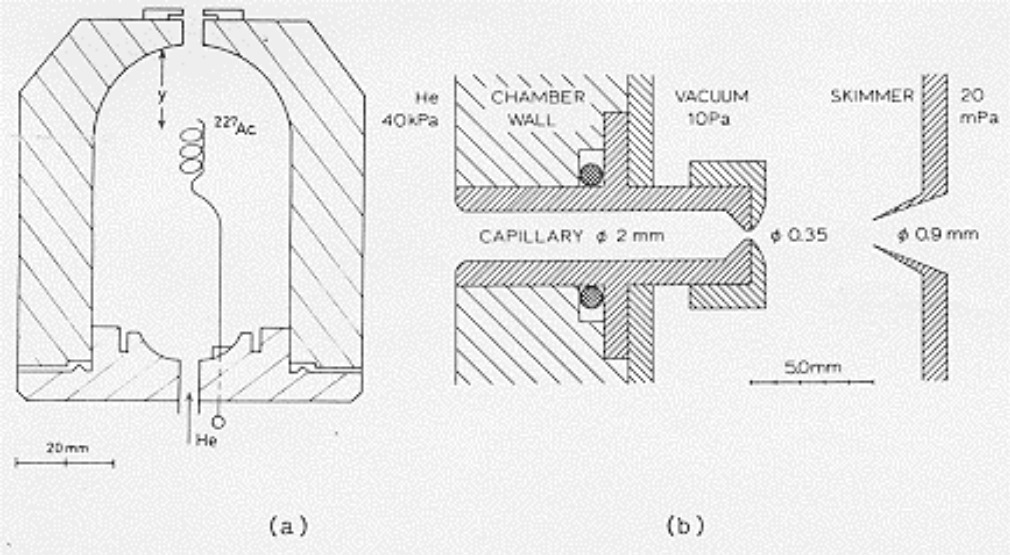

Fig. 3-9. (a) Recoil chamber of 75 cm^3 used in studies with the ^{227}Ac source, (b) capillary and skimmer in detail. [22]

following measurements where the yields of ions were studied. The reference value $\Sigma_o = 6500$ corresponds to the transport efficiency $\Sigma_o/N' \approx 5 \pm 2$ %, where N' is the number of particles recoiling from the source. The efficiency was measured by means of the method described in reference [105].

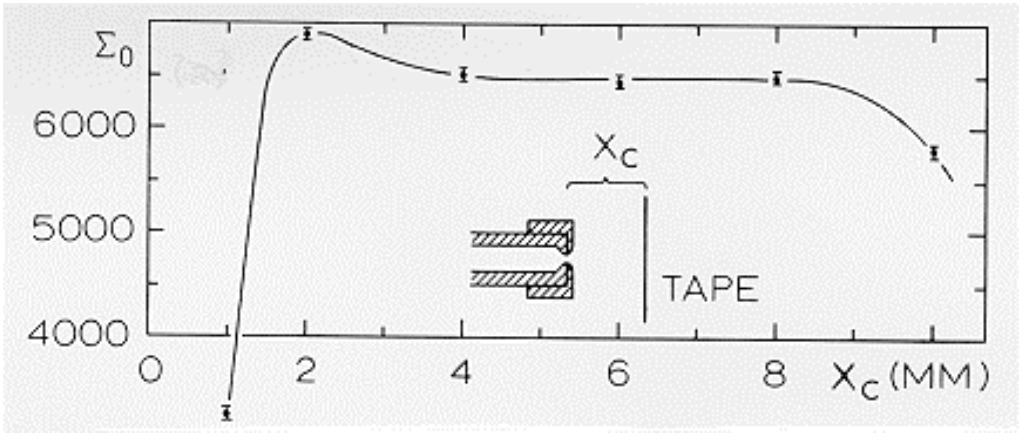

Fig. 3-10. The number of observed α disintegrations Σ_o as a function of the distance x_c between capillary and transport tape. [22]

The yield of recoil particles passing through the capillary is shown in fig. 3-11. The curve was measured with no voltage between the capillary and the transport tape. When increasingly negative voltages were applied to the source, the yield was quickly reduced below 5 per cent of its maximum value. This indicates that only a few per cent of the primary decay products are neutral particles or negative ions. When no voltage was applied across the chamber, the yield was still slightly below the maximum value. Evidently some recoils are adsorbed back onto the source because of their short range (R≈ 1 mm) and because of thermal diffusion. When a small positive voltage was applied to the source, it repelled the positive ions and the maximum yield was reached. The helium flow toward and through the capillary predominated, and the fraction of ions lost to the walls was minimal. At higher positive voltages the yield decreased again when the drift toward the walls increased. With voltages S≈>+15 V all ions were forced to collide to the walls inside the recoil chamber. This is indicated by a saturation of the yield curve. The difference between the two saturated curves is 10 per cent. Because the fraction of the recoils neutralized in wall collisions without adhesion cannot be deduced from the curves, the loss of ions during the transport from the source to the capillary inlet appears to be at most 10 per cent.

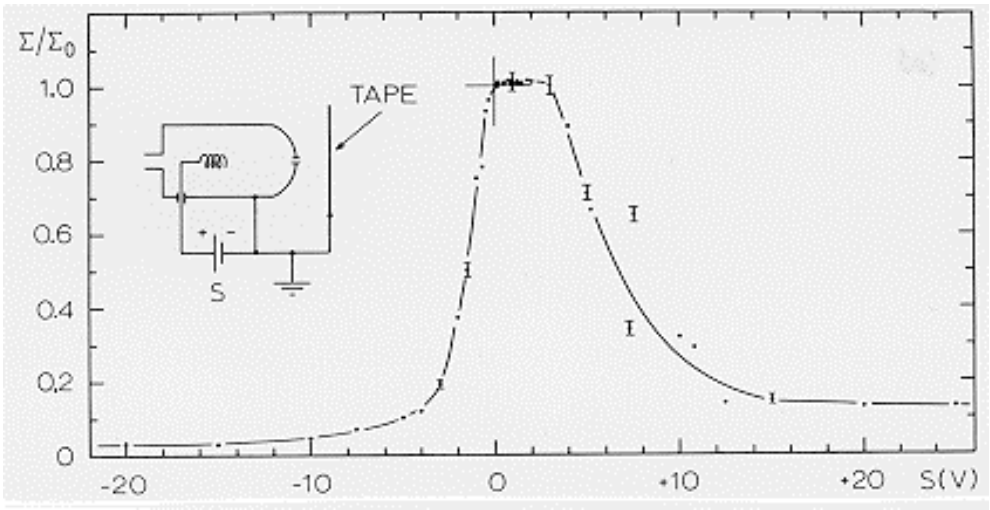

Fig. 3-11. The relative number Σ/Σ_0 of observed α disintegrations as a function of the potential difference S across the recoil chamber. Here x_c was 5 mm. [22]

The fraction of transported, positively charged recoil ions was studied with the arrangement shown in fig. 3-12. The retarding potential between the collector tape and the capillary exit prevented positively ionized particles from reaching the tape.

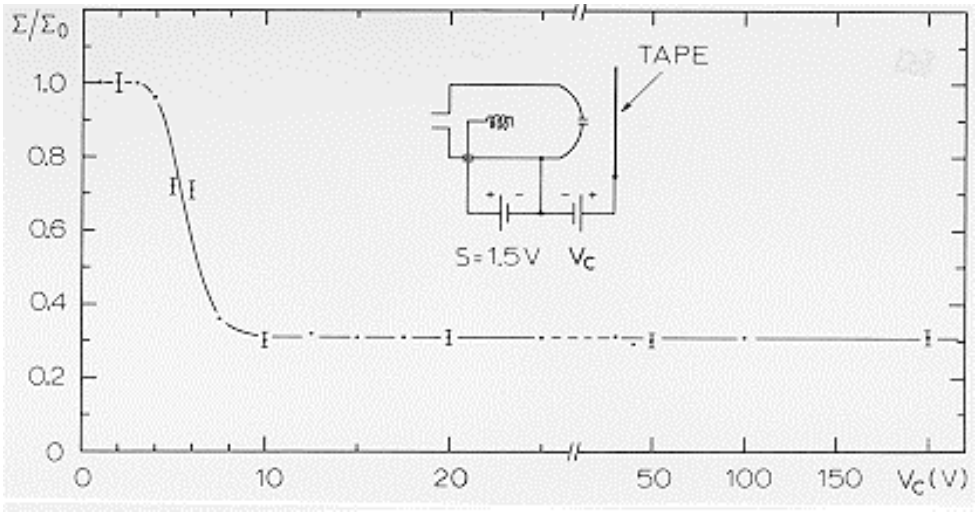

Fig. 3-12. The relative number Σ/Σ_0 of observed α disintegrations as a function of the potential difference V_c between capillary and collector tape. Here x_c was 5 mm. [22]

Between 3 and 10 V the relative number of α disintegrations observed was reduced from 100 per cent to 31 per cent, where it remained constant. This indicates that 69 per cent of the particles collected were positive ions. Comparing this result with that in fig. 3-11 reveals that the loss of ions during transportation through the capillary is at least 20%. The loss is mainly due to the diffusion of ions to the walls of the capillary. Between the capillary exit and the tape the loss of ions was assumed to be negligible. This interpretation was later supported by measurements where the capillary was replaced by an exit hole. In that measurement the ion guide parameters were changed to $V_{tc}\approx 20$ cm^3, $\phi_e=0.65$ mm and $p_{tc}=200$ mbar (the second row in table 3-3). The result of the measurement showed that 98 per cent of the decay products were prevented from adhering to the collector tape by the retarding voltage. This indicates that only two per cent of the collected decay products were

neutral particles or negatively charged ions when leaving the ion guide [23,24].

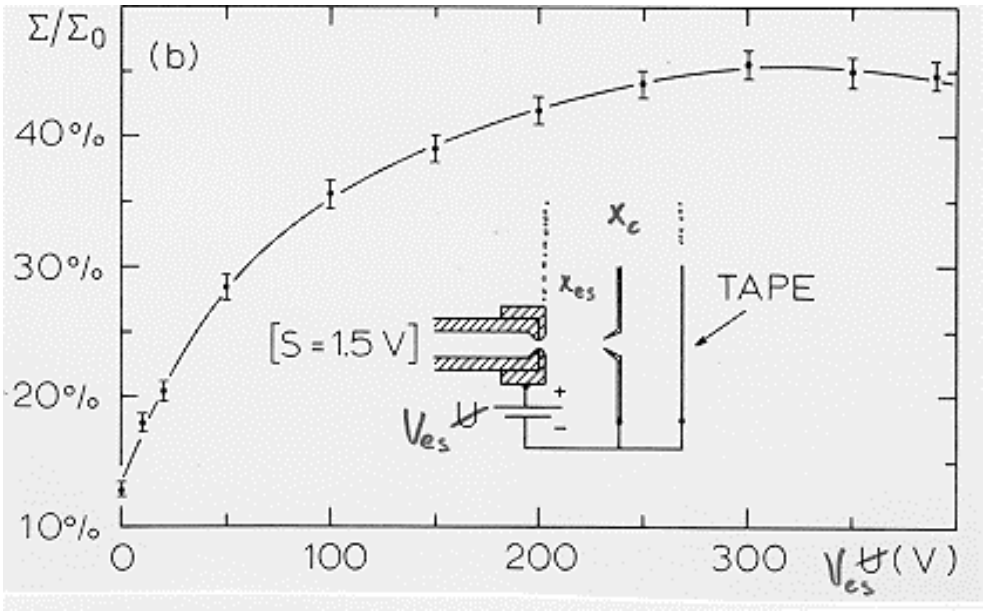

Fig. 3-13. The relative number Σ/Σ_o of observed α disintegrations as a function of the skimmer voltage V_{es}. The distances were x_c= 8 mm and x_{es}= 5 mm, and the diameter of the skimmer was ϕ_s= 0.9 mm. [22]

Fig. 3-13 shows an arrangement where the dependence of the yield on the skimmer voltage was studied. Without the voltage the relative yield was about 13 per cent and the highest transport efficiency, 45 per cent through the skimmer was achieved with the skimmer voltage -300 V.

3.2.2.3. Mass separation of primary recoil ions emitted from the ^{227}Ac source

To mass separate primary recoil ions from the ^{227}Ac source the ion guide chambers were connected directly to the accelerating stage of the isotope separator. The tape transport equipment was installed beside the collector chamber of the separator so that the collector tape was

perpendicular to the central radius of the mass separated ion beam. Using this arrangement, it was possible to focus only one mass at a time, since the focal plane deviates 24.1° from the one used.

The volume of the recoil chamber (fig. 3-14) was reduced to the value of 20 cm^3 by using a teflon cylinder inside the 75 cm^3 chamber. Also the capillary was replaced by an exit hole.

Using the smaller chamber, the system was faster and more effective. Furthermore, with mass separation, it was not necessary to wait for a decay of the ^{219}Rn in the recoil chamber any more: With the resulting kinetic energy of 40-50 keV, Rn-ions will penetrate deep enough into the collector tape and stay there for the time needed for detection of their α–decay.

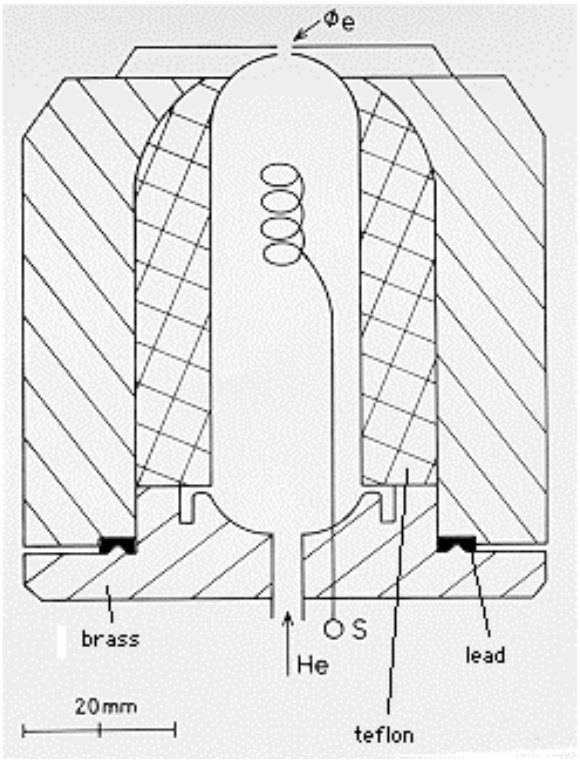

Fig. 3-14. The recoil chamber used in studies of characteristics of the ion guide isotope separator (IGIS). The parameters were V_{tc}= 20 cm^3 and ϕ_e= 0.65 mm. The distance between the recoil source and the exit was y= 20 mm.

In addition to better transmission of ions than that of the capillary, the second advantage in using the exit hole is that the latter produces a wider flow pattern of gas behind the exit of the recoil chamber. This reduces the amount of helium penetrating the separator. The maximum pressure in the extraction chamber was kept at the value of $\approx< 2x10^{-4}$ mbar.

Although the ions were spread over a fairly wide angle (≈50° at FWHM), with the skimmer voltage the ions could quite effectively be guided into the separator. The best mass separated yield of recoil ions was produced with the ion guide parameters ϕ_s= 0.75 mm, x_{es}= 3 mm and V_{es}= -1100V, in addition to those presented in the second rows of table 3-3.

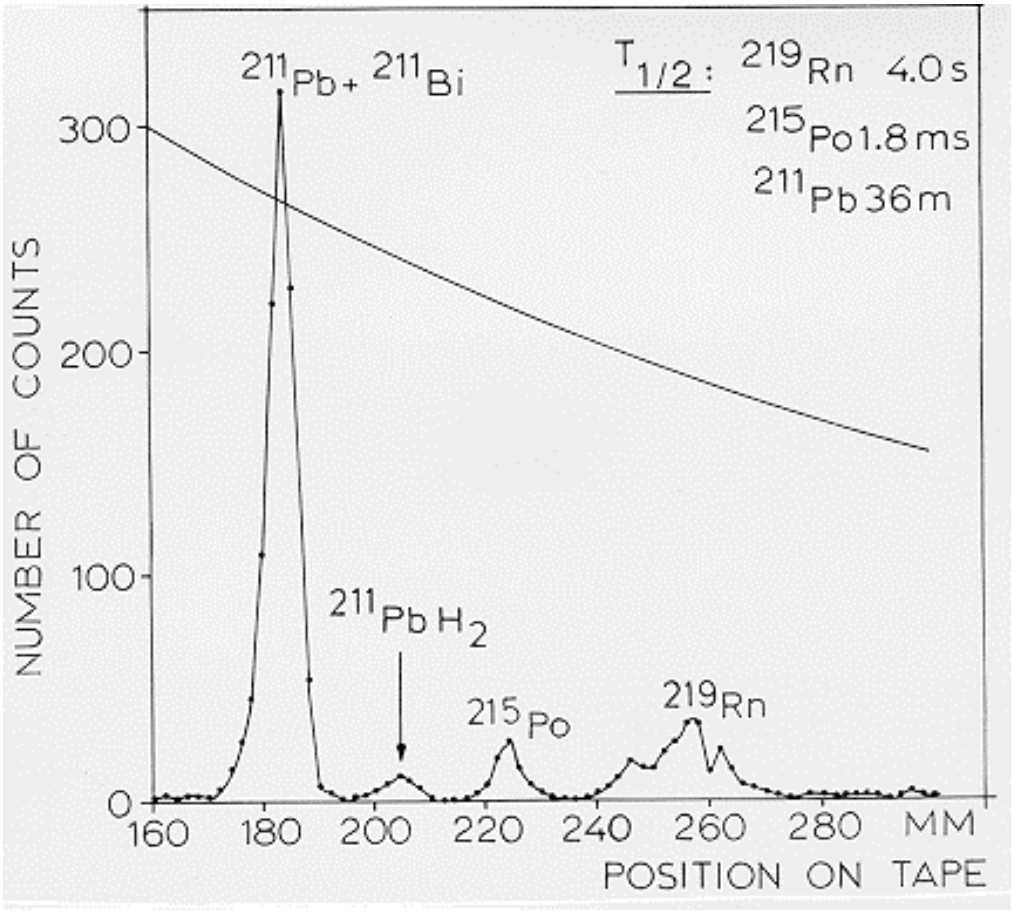

Fig. 3-15. Mass spectrum of the actinium series separated by the IGIS. The collection time of activity was 30 min and it was measured

afterwards as the α–activity of ^{211}Bi. No corrections have been made for decay during collection and measurement. The decay curve of 36 min ^{211}Pb gives a qualitative idea of the decay rate during measurement. [23]

The mass distribution of collected ions on the transport tape is shown in fig. 3-15. In this experiment the collection time of activity was 30 min, after which the tape was moved in 2 mm steps. At each position the measuring time of the α–activity of ^{211}Bi was 30 s. The effective area of the Si(Au)-surface barrier detector was 20 mm^2 being determined by the 2 mm wide and 10 mm high slit.
Using this arrangement, α–decays from other parts of the tape were eliminated.

The mass spectrum showed the charge states of the recoil ions to be +1 and the main part of the particles to be in atomic form. The weak peaks at mass positions A_i= 213 and 227 were found by an activity analysis to be $^{213}(PbH_2)^+$ and $^{227}(PbO)^+$ molecular ions. Doubly charged ions were not found in the mass separated samples.

The resolving power of 340 at the FWHM was determined from the focused mass A_i= 211.

The efficiency of the ion guide can be determined as a product

$$\varepsilon = \varepsilon_1 \cdot \varepsilon_2 \cdot \varepsilon_3 \ , \qquad (3.8)$$

where ε_1 = helium-jet efficiency,
ε_2 = fraction of positive ions among the transported particles
ε_3 = skimmer efficiency.
The following efficiencies were measured,

$$\varepsilon_1 = 20 \pm 5\ \%,$$
$$\varepsilon_2 = 95 \pm 5\ \%,$$
$$\varepsilon_3 = 66 \pm 5\ \%.$$

The resulting efficiency calculated from these figures is

$$\varepsilon = 13 \pm 5\ \%.$$

The error limits are based on repeated experiments. The value of the efficiency is valid for half-lives longer than about 0.1 s, which corresponds to the evacuation time of the recoil chamber.

As an example, fig. 3-16 presents the result of one of the measurements where the time dependence of increase of mass separated activity (^{215}Po, $T_{1/2}$= 1.8 ms) was studied. The increase was determined by pulsing the source voltage S: with S ≈< -15 V the mass separated yield was zero (refer to fig. 3-11) and with S ≥ 0 V the yield increased with time and was finally saturated to its maximum value. In this example one measurement lasting 4 seconds, was repeated 340 times. The source was 'on' for two seconds for activity separation and 'off' for the next two seconds to measure the background. Due to the spiral shape of the source wire, the electric field inside the recoil chamber was not geometrically optimal. This reflected to the benefit of the field.

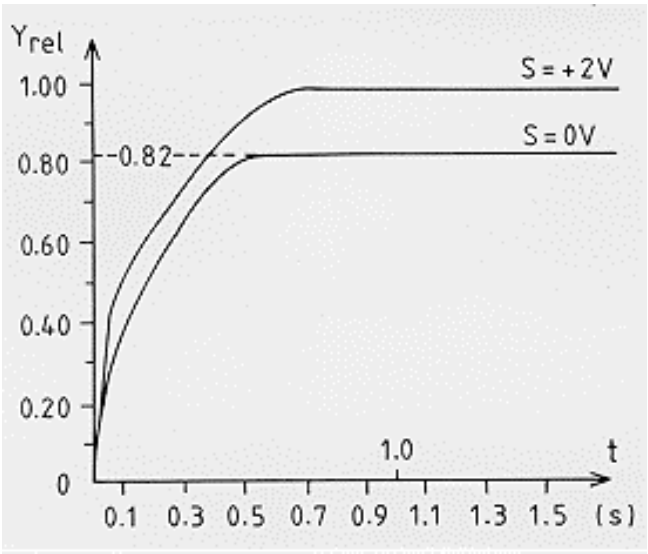

Fig. 3-16. Growths of relative yields of the mass separated ^{215}Po as a function of time at p_{tc}= 200 mbar. The voltage across the recoil chamber was S= +2 V and S= 0 V. The yields are normalized to the saturated value with S= +2 V.

The only clear effect found was the better yield with the voltage. The saturation times of the curves did not correspond to the calculated evacuation time of the recoil chamber (≈0.1 s), because the situation is rather complex at the moment the source is switched 'on': The parent of the separated activity, radon being an inert gas , fills the whole chamber volume and the final result is thus influenced by distributions in transportation, diffusion, drift and decay.

3.3. *On-line experiments*

The nuclei used in on-line development work and experiments were produced via p, d, ^{3}He and α induced reactions by bombarding solid and gaseous targets (0.1-5 mg/cm^2) with the beams from the mini-cyclotron at the Department of Physics, University of Jyväskylä (JYFL). The number of reaction products used in investigations was 39 produced from 16 solid targets and one gaseous (Ne) target [26].

Most of the on-line development work has been done by using the reactions

$$^{54}\mathrm{Fe(p,n)}^{54}\mathrm{Co}\ , \quad T_{1/2} = 193\ \mathrm{ms}$$

and

$$^{\mathrm{nat}}\mathrm{Zn(p,n)}^{64}\mathrm{Ga}\ , \quad T_{1/2} = 2.62\ \mathrm{min.}$$

The former has been used in mass separation tests. The other reaction was useful when the yields of radioactive recoil ions were studied at the skimmer position. The latter experiments were carried out at the Cyclotron and Radioisotope Center (CYRIC) of Tohoku University in Sendai, Japan.

3.3.1. Experimental facilities

The properties of the accelerators in Jyväskylä and in Sendai are briefly described in table 3-5. In addition to light ion beams, ^{14}N and ^{16}O light heavy ion beams are also available at CYRIC.

The properties of both separators and the ion guides are almost equal [26,27,107], the only bigger differences being in pumping capacities. At CYRIC two Roots blowers (800 l/s and 200 l/s) are connected in series with a rotary vane pump that gives a better pumping of the vacuum chamber than that at JYFL (Roots 555 l/s). On the other hand the pumping speed in the extraction chamber is a little lower at CYRIC, being ≈500 l/s as compared with ≈650 l/s at JYFL.

The higher pumping capacity in the vacuum chamber of the Tohoku IGISOL makes possible the use of a larger skimmer hole, ϕ_s= 2.0 mm.

Further, in both laboratories the original volumes of the target chambers, ≈20 cm^3, have been subsequently reduced by using aluminium plugs inside the chambers. The volumes V_{tc}≈ 1-2 cm^3 with ϕ_e= 1.2 mm seem to yield radioactive recoil ions for injection into the separator most effectively.

Particle	E_p (MeV)		$I_{p,max}$ (pμA)	
	K=20 MeV	K=50 MeV	K=20 MeV	K=50 MeV
p	5-20	3-40	1.5	10
d	6-10	5-25	1.5	5
^{3}He	12-27	7-65	0.2	5
α	6-20	10-50	0.2	5

Table 3-5. Properties of the cyclotrons at JYFL (K= 20 MeV) in Jyväskylä and at CYRIC (K= 50 MeV) in Sendai, Japan. See ref. [106].

The radioactivities of the separated nuclides were detected by conventional methods including: Si(Au)-surface barrier detectors for beta-delayed particles, Si(Li) and plastic scintillator detectors for beta-rays, Ge(Li) and Ge(HP) detectors for gamma-rays. Various tape transport systems in the collection chamber of the separator were used for activity transportation. The half-lives of the shortest lived nuclei (<100 ms) were determined using periodic electrostatic deflection of the separator ion beam.

3.3.2. The effect of buffer gas pressure on the yield of radioactive ions

Dependence of the yield of recoil ions on buffer gas pressure was studied by using the reaction ^{nat}Zn(p,n)^{64}Ga. The measurements were made without mass separation, because the highest flow rates used did not allow coupling to the isotope separator. The half-life of ^{64}Ga, $T_{1/2}$= 2.62 min, is long enough for collecting the activity at the skimmer

position and for transferring it to a low background area where measurement can take place. The projectile energy 16 MeV gives the highest cross-section of ≈300 mbarn for this reaction [108,109]. The collection and measurement times were 10.5 min and 10 min, respectively, with a time interval of 3 min between them.

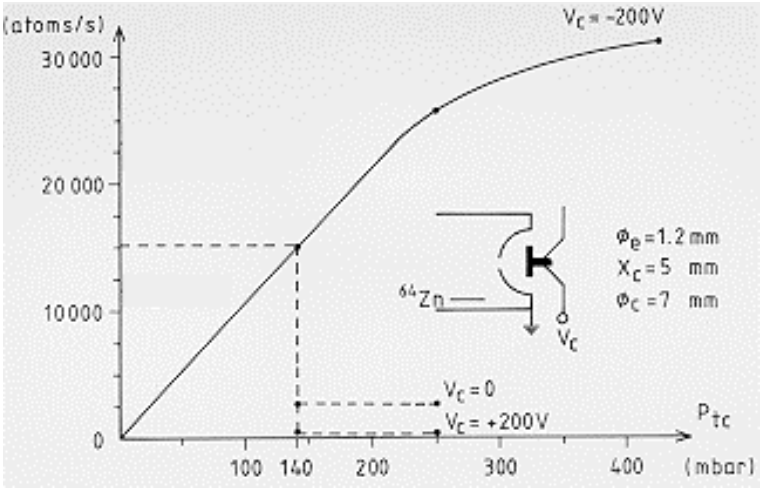

Fig.3-17. Absolute yields of recoil atoms ^{64}Ga as a function of helium buffer gas pressure, measured with three different voltages (V_c) between target chamber exit and collector. The yields are normalized to correspond to an enriched ^{64}Ga target and to 1 μA proton beam intensity. The arrangement of the measurement is shown in the insert. The dashed line at p_{tc}= 140 mbar corresponds to the maximum target chamber pressure which present pumping speed in the extraction chamber permits.

A motive for this study was to learn, how the yield of recoil ions behaves at higher gas pressures than presently possible in the IGISOL experiments. Under these conditions three-body recombination becomes more probable due to an increased plasma density [80,85]. On the other hand, ionization of neutral recoil atoms due to helium ions and metastable He atoms becomes more probable, too. Perhaps the most important change is that the transport conditions are improved; the stopping efficiency increases with increasing pressure and the losses due to diffusion to the chamber walls are reduced.

Figure 3-17 shows an arrangement and the result of the measurement. The yields of recoil ions were determined by using electric potentials between the exit hole and the Al-collector plate. The measurements were carried out at pressures of 140, 250 and 425 mbar. The diameters of the exit hole and the collector plate were 1.2 mm and 7.0 mm, respectively, and the distance between them was 5 mm.

Three different voltages V_c= -200, 0 and +200 V were used. At each voltage the collection efficiency of neutrals was equal, while with the negative voltage on the collector, positive recoil ions were accelerated towards the plate, and negative ions were repelled from it. Using the positive voltage the situation was reversed. At the pressure p_{tc}= 425 mbar the yield was measured only with V_c= -200 V.

The results in fig. 3-17 are normalized to correspond to an average recoil range in an enriched ^{64}Ga target, bombarded with a 1 μA beam intensity. The amount of negative ions appeared to be negligible. The collection efficiency of neutrals was also very low. An increase in pressure didn't increase the total yield of neutral particles. Also the result reveals that positive ions are collected more effectively than neutral atoms when no external fields are applied.

The yield of positive ions increases linearly up to the pressure of 250 mbar above which it seems to saturate. Theoretically the stopping efficiency in the buffer gas reaches a value of 100% at 250 mbar, assuming the recoil energy of 3.9 keV/u.

The calculated total yield of ^{64}Ga atoms recoiling out of the target is 1.39×10^6 atoms/s. This means that the maximum collection efficiency in these experiments was 2.2%.

The most important result which can be deduced from these measurements is that the ion guide has capacity to produce more ions than can be presently (see dashed line in fig. 3-17) injected into the separator.

3.3.3. Mass calibration and focussing with stable ions - properties of the IGISOL ion beams

When a projectile beam passes through the helium-filled target chamber, some helium atoms and impurity molecules are ionized in collisions with projectile particles. Additional ionization of the gas is caused by delta electrons from the target and the windows of the target chamber as well as from the buffer gas.

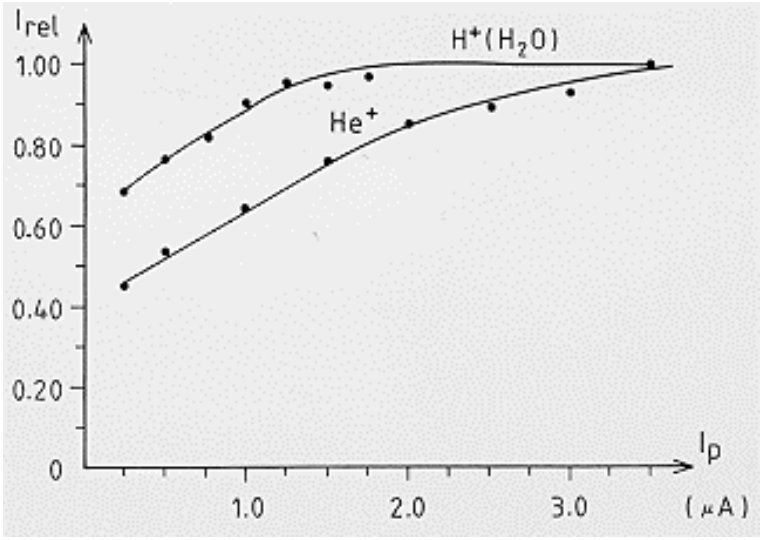

Fig. 3-18. The relative current of the mass separated stable ions He^+ and $H^+(H_2O)$ as a function of the intensity of the 30 MeV proton beam.

The stable molecular ion beams provide a built in mass calibration and a means for focussing the IGISOL ion beams. The degree of ionization or plasma density has not been measured. However, the experimental result shows that 1 μA proton beam induces about 1 μA ion beam emerging out of the target chamber when 100 mbar pressure and 1.2 mm exit hole are used. Increasing the intensity of the projectile beam increases the total ion beam almost linearly.

The behaviour of individual molecular ion beams can be quite different as demonstrated in fig. 3-18, where stable ion beam intensities are presented for mass numbers A_i= 4 and 19 as a function of the 30

MeV proton beam intensity. The saturation of the cluster ion current of $H^+(H_2O)$ after ≈2 μA proton beam is not well understood.

Figure 3-19 shows a typical mass spectrum of molecular ions. The spectrum has essentially the same appearance as the one induced by the spark discharge ion source. Small differences in intensity ratios between individual masses can be found. The mass calibration and the focussing of the IGISOL for masses heavier than A_i= 52 are made by means of a small amount of Kr or Xe gas mixed within helium or by a small drop of Hg added into the target chamber. The former for the mass region A_i≈ 100 and the latter for A_i≈ 200.

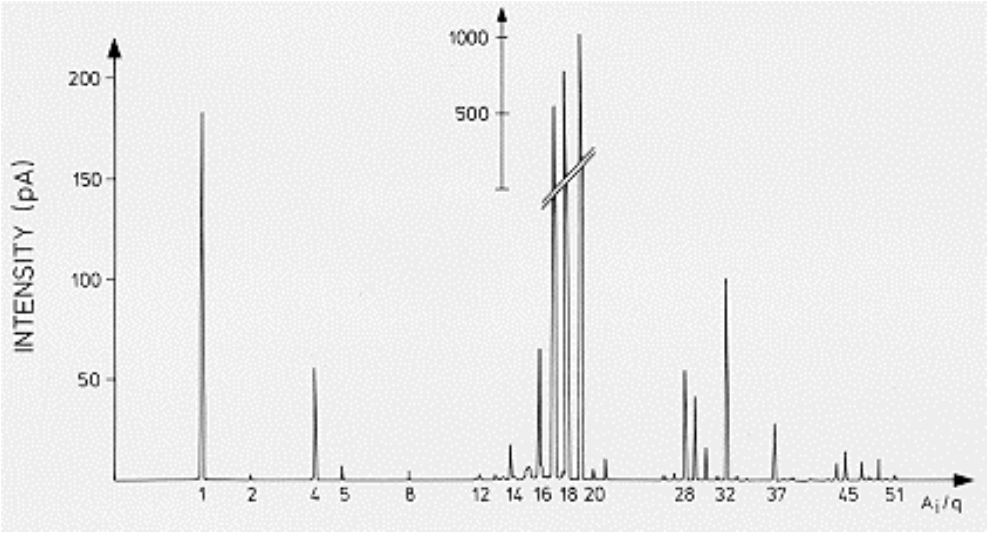

Fig. 3-19. Mass spectrum of stable ions induced by a proton beam.

The most critical parameter for the mass resolution of the IGISOL is the helium pressure between the exit of the target chamber and the extraction electrode of the separator. In typical on-line conditions (see table 3-1) the resolving powers (RP) in the mass region A_i≈ 50 are (fig. 3-20),

$$RP_{0.5} = A_i/\Delta A_{0.5} = 375 ,$$
$$RP_{0.1} = A_i/\Delta A_{0.1} = 200 ,$$

where ΔA is the full width of mass A_i at the height of 0.5 or 0.1.

The value of magnetic bending for an ion with the charge of +1, the energy of E_i and the mass of A_i is

$$B\rho = 4.55 \times 10^{-2} (E_i A_i)^{1/2} , \qquad (3.9)$$

where B is the strength of the magnetic field in kG, ρ is the radius of curvature in m and E_i and A_i are the energy and mass of the ion in keV and u, respectively.

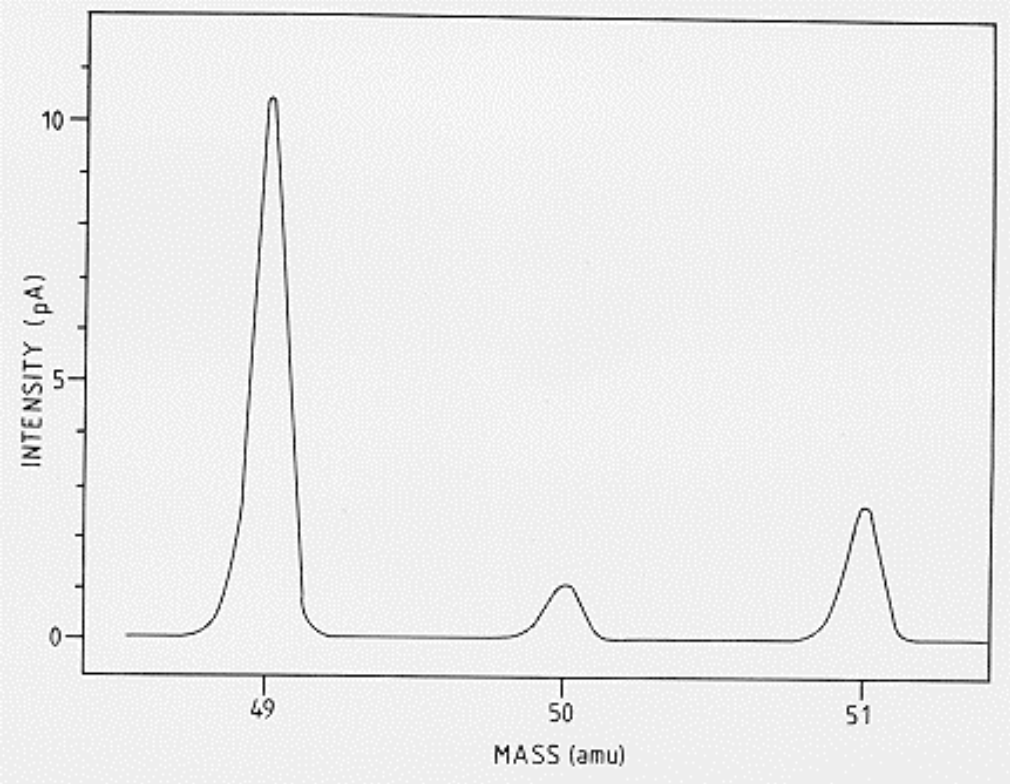

Fig. 3-20. An expanded section of the mass spectrum at mass region A_i= 50. [26]

Using eq. 3.9 with the measured values of B= 1.328 kG and E_i= 40 keV and the above values for resolving powers, the calculated energy dispersion ΔE of the IGISOL is found to be

$$\Delta E_{0.5} \approx 100 \text{ eV} \quad \text{or} \quad \Delta E/E \approx 2.5 \times 10^{-3} ,$$

$$\Delta E_{0.1} \approx 200 \text{ eV} \quad \text{or} \quad \Delta E/E \approx 5 \times 10^{-3}$$

at the mass region $A_i \approx 50$.

The energy loss of ions due to their acceleration through relatively high pressure helium between the exit hole and the extraction electrode was found to be of the order of 5 per mille of the total extraction energy given by the skimmer and extraction voltages together.

3.3.4. Comparison of the yields of radioactive ions thermalized in He, Ne, Ar and N_2 buffer gases

The dependence of yields of radioactive recoil ions on the type of buffer gas was studied using noble gases helium, neon and argon, and a molecular gas nitrogen. The test reaction was $^{27}Al(p,n)^{27}Si$, where the half-life of the reaction product is $T_{1/2} = 4.2$ s. The projectile energy was 16 MeV and a constant beam current of 0.5 μA was used. Because buffer gases other than helium and neon would cause high voltage instabilities in the Roots pumping line (Roots was in ground potential) and in the extraction section of the separator, a low accelerating voltage (≈5 kV) in the separator had to be used. For this reason, no mass separation was made and the collection of activity took place on a foil in front of the analyzing magnet. A small collection chamber with a ß-detector was installed between the accelerating chamber and the magnet of the separator.

Transport yields of recoil ions are mainly determined by the four factors: stopping power of the gas, diffusion of ions in the gas, recombination of ions in the target and in the gas phase and ionization of neutral recoils in gas.

Survival of thermalized ions is related to the ionization potential of buffer gas atoms, so that in gases with higher ionization potentials electron capture cross-sections are smaller (ch. 2.1.3.).

Element	I_B (eV)	Rp (mbar-cm)	ε_{stop}	τ_{Da} (ms)	n_i/n_n ($x10^{-7}$)
Si-recoil	8.9				
He	24.6	713	0.14	4.3	1.2
Ne	21.6	230	0.44	11	3.1
Ar	15.8	172	0.58	32	3.7
N_2	15.6	141	0.71	41	7.7

Table 3-6. Properties of different buffer gases related to survival of recoil ions in the target chamber of the IGISOL. See explanations in the text.

Exceptionally small cross-sections have been found in helium, where a reversed effect is possible; ionized recoils may be created during the thermalizing process (ch. 2.1.2).

Table 3-6 presents some properties of buffer gases which control the survival of ^{27}Si recoil ions. The second column shows the ionization potentials of silicon and gas atoms. The stopping properties of the buffer gases are calculated in the third and fourth columns using equations presented in chapter 2.2 and reference [90]. The average recoil energy was estimated to be 21.2 keV/u. The stopping efficiency of the gas corresponds to the stopping distance x= 1 cm and the pressure p_{tc}= 100 mbar. Average diffusion times of recoil ions to the chamber walls are calculated from ambipolar diffusion coefficients which have been estimated from the experimental mobility values of Si ions (or of ions with the same properties) in those gases [99,110]. Here the ambipolar diffusion coefficient is assumed to be $D_a = 2D_i$. In the last column the degree of ionization of the buffer gas induced by the proton beam is calculated using the ionization cross-sections that appear in ref. [77]. Due to the lack of data, the rate coefficients of three-body recombinations of Si ions in gases are not included in the table.

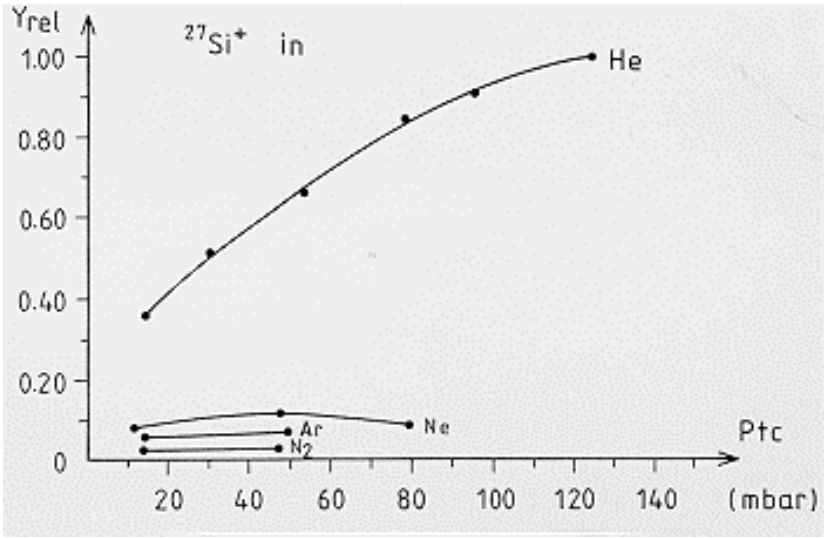

Fig. 3-21. Relative yields of the ^{27}Si recoil ions thermalized in He, Ne, Ar and N_2 buffer gases.

Figure 3-21 shows the experimental results in the four cases. The yields represent the relative, saturated values of the detected ß-particles which were emitted from the collected ^{27}Si ions. When the experimental results are compared with the properties of the gases presented in table 3-6, it can be deduced that the survival of recoil ions during their transfer from high-pressure thermalizing volume to low-pressure detection area is related to reactions of the ions with buffer gas atoms or molecules and with free electrons. For example, about five times more recoils are stopped in nitrogen than in helium, but only a few per mille of recoils can be transported in ionized form with the former gas. Also the losses due to diffusion are negligible in nitrogen. In every case the evacuation time of the target chamber was about equal, being in millisecond region. Whether the result represents the general behaviour of recoil ions in the ion guide, has still to be verified with other reaction products.

3.3.5. Mass separation of radioactive recoil ions

3.3.5.1. Injection of ions into the separator

For injection of recoil ions into the accelerating stage of the separator optimal values for distance between the exit and the skimmer and for the diameter of the skimmer hole have to be found. In addition final tuning has to be made by the skimmer voltage.

The results presented in the previous chapters showed that the yield of ions increased with the increasing pressure (figs. 3-17 and 3-21). A practical lower limit for the pressure in the target chamber is ≈50 mbar, which still ensures a satisfactory yield of recoil ions. With lower pressures stopping efficiencies are so small and diffusion times to the chamber walls so short that large losses of ions will take place. The evacuation time of the target chamber has to be balanced with the stopping efficiency and diffusion. The parameters of the target chamber under optimum conditions are more or less fixed to the values, $V_{tc} \approx 1$ cm^3, $\phi_e = 1.2$ mm and $p_{tc} > 50$ mbar.

In principle, the amount of recoil ions injected into the separator is proportional to the area of the skimmer hole and inversely to the skimmer distance. According to the previous results, it also depends on the pressure in the target chamber and on the skimmer voltage. The number of radioactive ions Y^+ injected into the separator can be described by the empirical relation,

$$Y^+ \propto (\phi_s)^2 / x_{es} \; p_{tc} \; f(V_{es}) \; , \qquad (3.10)$$

where $f(V_{es})$ represents the dependence of the skimmer transmission on the skimmer voltage.

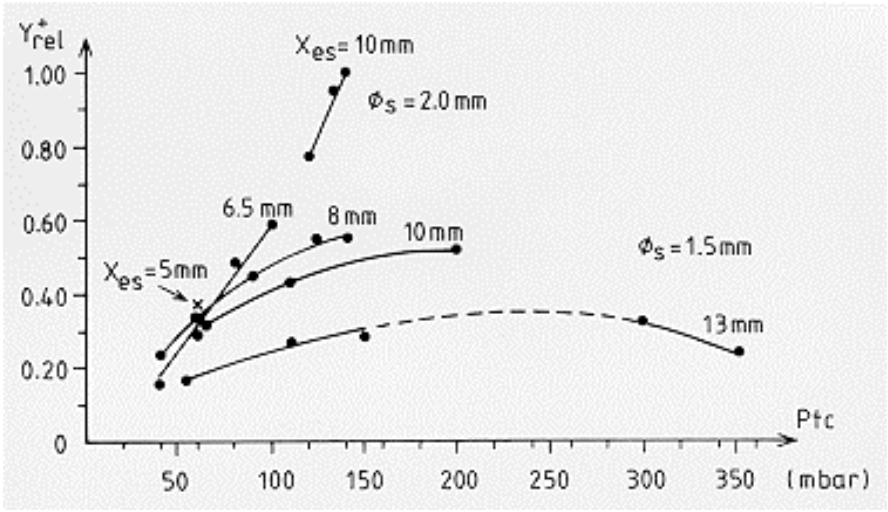

Fig. 3-22. Relative yields of ^{64}Ga ions with the parameters ϕ_s= 1.5 mm and ϕ_s= 2.0 mm as functions of x_{es} and p_{tc}. The relative yield 1.00 corresponds to 16500 ions/s with the beam intensity I_P = 1 μA.

In practice, the vacuum conditions in the extraction chamber of the separator finally determine the optimal values of the parameters in eq. 3.10. As already mentioned, the maximum value of the helium pressure has been found to be $p_{ext}(max) \approx 2x10^{-4}$ mbar, as measured above the baffle of the diffusion pump. At higher pressures the energy dispersion of the IGISOL ion beam increases rapidly.

Figure 3-22 presents the dependence of the ^{64}Ga recoil ion yield on the target chamber pressure with different values of skimmer distance and diameter. In each case the best value for the skimmer voltage has been used. The upper end point of each curve corresponds to the value of $p_{ext} \approx 2x10^{-4}$ mbar. The best yield with the 1.5 mm diameter skimmer was found at the position x_{es}= 6.5 mm with p_{tc}= 100 mbar and V_{es}= -500 V. The throughput of helium at 100 mbar pressure was 65 mbar l/s. A significant increase in the yield was found after the skimmer diameter was increased to 2.0 mm. The optimum distance for this skimmer was 10 mm. Here at the highest pressure of 140 mbar (Q≈ 90 mbar l/s) the skimmer voltage -1000 V gave the best yield.

The steep slope of the curve reveals the necessity of a higher pumping capacity in the extraction chamber. This was clearly demonstrated by the fact that when the pressure in the target chamber

increased by a factor of 1.17, from 120 to 140 mbar and the yield at the same time increased by a factor of 1.30, the corresponding increase in the extraction chamber pressure was as high as 2.5. An interesting feature of the curves in fig. 3-22 is that at optimum conditions the increase in the yield is linear with increasing pressure.

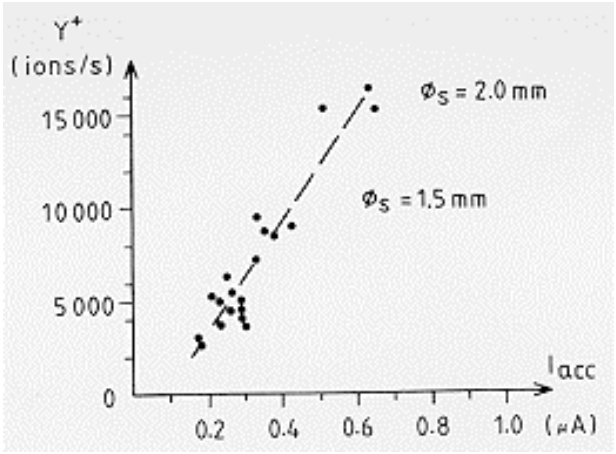

Fig. 3-23. Relation between yields of radioactive ions ($^{64}Ga^{+}$) and total currents of stable molecular ions. The yields correspond to the results presented in fig. 3-22. I_{acc}= total accelerated ion current in front of the analyzing magnet.

The quality of the phenomenological relation 3.10 under optimal conditions is well demonstrated by the present results: The measured change in the yield when going from the 1.5 mm diameter skimmer to the 2.0 mm skimmer is a factor of 1.71, and the calculated change is 1.62. The calculated results correspond to the optimal skimmer voltages where it is used $f(V_{es})= 1$.

Figure 3-23 demonstrates the relation between yields of radioactive ions and stable ion current. The latter was measured as the total current of positive ions in front of the analyzing magnet. Roughly the trend is the following: higher currents of stable ions indicate higher yields of radioactive ions.

3.3.5.2. Dependence of the yield on the projectile beam intensity

When the intensity of the projectile beam passing through the target chamber is increased, the amount of thermalized, radioactive recoil ions is naturally increased. But at the same time, the degree of ionization in the buffer gas is increased, too. As a consequence of denser plasma, three-body recombinations of recoil ions with electrons in the gas become more probable, which may reduce the amount of recoil ions. Also the average temperature of electrons becomes higher which may cause larger ambipolar diffusion rates, resulting in more losses of ions to the chamber walls. In order to find out if these phenomena affect or appear in the present operating conditions and how they are related to specific ions, three different (p,n)-reactions were studied,

$^{54}Fe(p,n)^{54}Co$, $T_{1/2} = 193$ ms,
$^{58}Ni(p,n)^{58}Cu$, $T_{1/2} = 3.2$ s,
$^{nat}Zn(p,n)^{64}Ga$, $T_{1/2} = 2.6$ min.

In the first reaction the projectile energy was 16 MeV and the proton current varied from 0.1 to 1.0 μA. In the latter two reactions the energies were 15 MeV and the currents from 0.14 up to 4.4 μA for ^{58}Cu and 0.5-2.5 μA for ^{64}Ga. In each case the ion guide parameters were equal (table 3-1), with the constant pressure p_{tc}=100 mbar.

Figure 3-24 presents the behaviour of the recoil ion yields as a function of the proton beam intensity. The yields are actual ß$^+$-counting rates (background subtracted) from the mass separated samples. In the first reaction the yield increased linearly with the beam current. In this case it was not possible to study how the yield would behave with higher proton currents, but on the basis of the measured points, it can be concluded that the possible saturation of the yield should be far above 1 μA beam intensity.

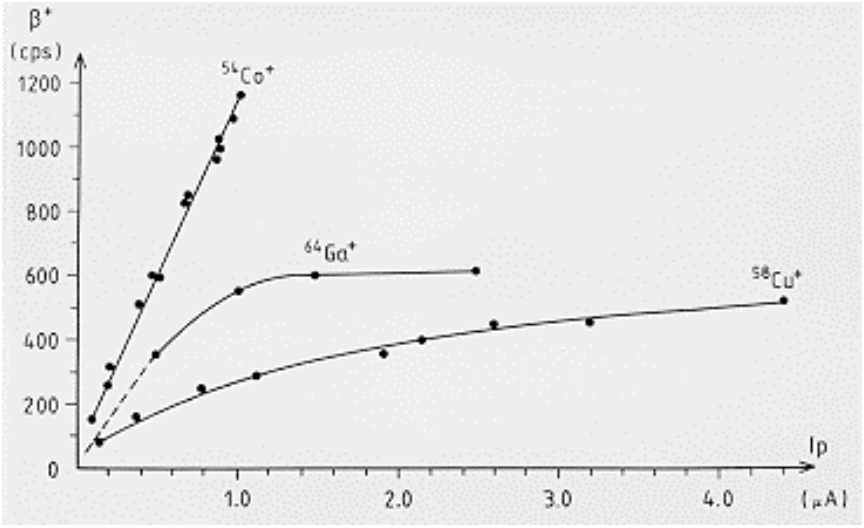

Fig. 3-24. ß+-counting rates of mass separated $^{54}Co^{+}$, $^{58}Cu^{+}$ and $^{64}Ga^{+}$ ions as a function of the proton beam intensity.

In the second reaction the yield also increases with increasing proton current, but not so linearly as in the first reaction. The yield from the third reaction, however, clearly saturates after $I_p \approx 1$ μA. The different behaviour of $^{64}Ga^{+}$ under the same conditions as the other two recoils studied, suggests that there is another or are other mechanisms than those mentioned above, which cause losses of $^{64}Ga^{+}$ ions.

In conclusion, it was found that different elemental ions behave in different ways when the plasma density is increased in the buffer gas . It is difficult to point at any particular mechanism which control the yield of specific ions in those conditions. One additional fact is that parallel to increasing plasma density the density of neutral molecules decreases - contrary to the recoil ion yield. It follows that charge transfer reactions between doubly charged recoil ions and molecules become less probable. This should result in an increasing amount of doubly charged recoil ions.

3.3.5.3. Overall efficiency and transporting time of ions in the IGISOL

The overall transport efficiency and transport time in the IGISOL have been measured by producing nuclei with short-lived isomeric states and also by producing short-lived nuclei decaying through ß-decays. The

mass separated yields have been compared to the number of atoms recoiling out of the target.

In the case of the isomeric activities the total yields of recoils from the target were determined experimentally in-beam by observing the intensity of the delayed γ-rays de-exciting the isomeric state between the micro pulses of the cyclotron beam and by normalizing the observed intensity to the target thickness corresponding to the average range of recoils.

For the ß-decaying nuclides the cross-sections of the reactions were calculated by the ALICE code [111]. The recoil ranges in the target, as in the former case, were calculated by the semiempirical method of Biersack (ch. 2.2). The mass separated yields include corrections for the detection efficiency and for the background. Due to calculations of cross-sections and ranges, and due to an estimate of the detection geometry, the accuracies of the overall efficiencies are assumed to be within a factor of two.

The overall efficiency for several nuclides as a function of the half-life is given in fig. 3-25. The efficiencies are the following:

$$\varepsilon_o \approx< 1\ \% \ , \quad T_{1/2} \approx< 400\ \mu s \ ,$$
$$1 \approx< \varepsilon_o \approx< 10\ \% \ , \quad T_{1/2} > 400\ \mu s.$$

With the exception of ^{90m}Nb this figure is limited to the mass region of 200 in order to avoid an additional mass-dependent factor on the efficiency, i.e., the loss of recoils to the chamber walls due to inadequate stopping in the gas. The absolute efficiency decreases with the increasing range, because the maximum usable gas pressure ($p_{tc} \approx$ 100 mbar) is limited by the present pumping capacity in the extraction chamber of the separator. For the isotope ^{90m}Nb the calculated stopping efficiency is $\approx$0.57. For other nuclides investigated the helium pressure is high enough to thermalize them in the gas phase. An open circle above the ^{90m}Nb in fig. 3-25 corresponds to the efficiency normalized to the value of $\varepsilon_{stop} = 1$. The efficiency curve starts to decrease below half-lives of about 4 ms. The decrease is related to the evacuation time of the target chamber in comparison to the half-lives of the nuclides. If the

efficiencies of the shortest lived nuclides observed, ^{207m}Bi (182 μs) and ^{202m}Tl (570 μs) were corrected with respect to the losses due to the relatively long transport time, their efficiencies would be 4.2 and 2.6 % (open circles in fig. 3-25), respectively. Because the diffusion rates of different ions in helium are nearly equal, the related losses should represent about same fractions in any reactions.

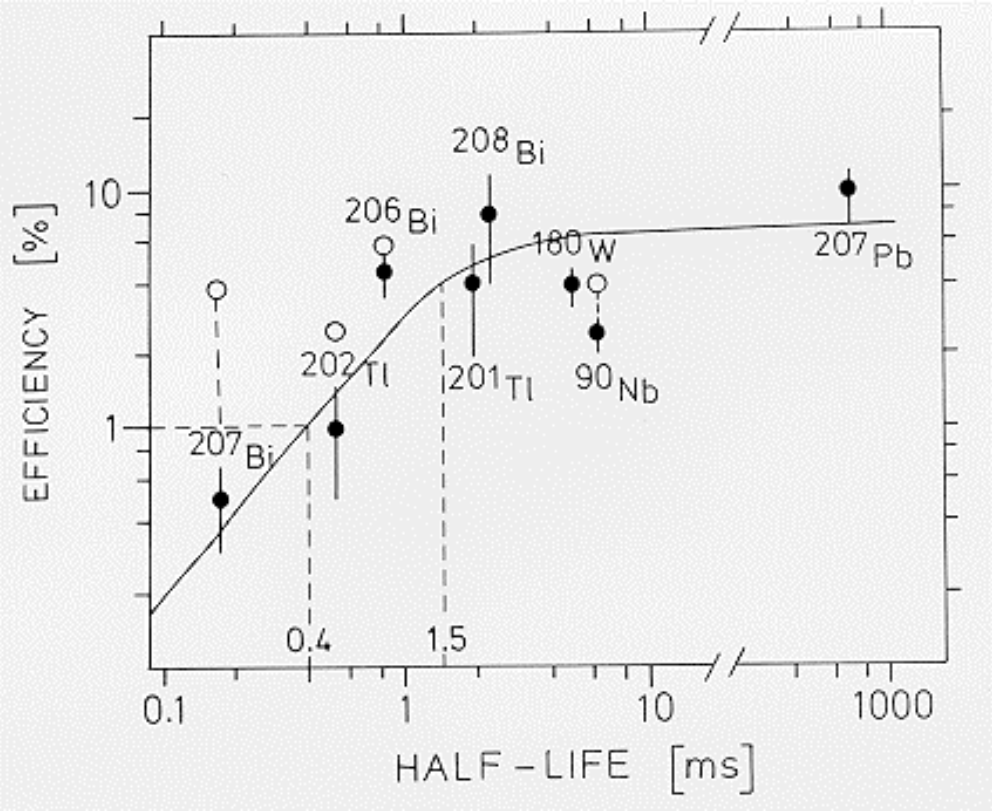

Fig. 3-25. Overall transmission efficiency for some heavy nuclides in their isomeric states as a function of half-life. The error bars are due to statistical uncertainties in the measurements. The open circles correspond to efficiencies corrected in respect to the evacuation time of the target chamber for ^{207}Bi, ^{202}Tl and ^{206}Bi, and to the stopping efficiency for ^{90}Nb.

Finally the correction of the efficiencies with respect to losses due to long ranges and to the transport time, indicate that the overall transport efficiency is between 1 and 10 per cent.

A remarkable finding is that the mass separated fraction of the activity does not seem to be too sensitive to the degree of volatility of the element, as is demonstrated by the good transmission of ions of the most refractory element, tungsten (fig. 3-26).

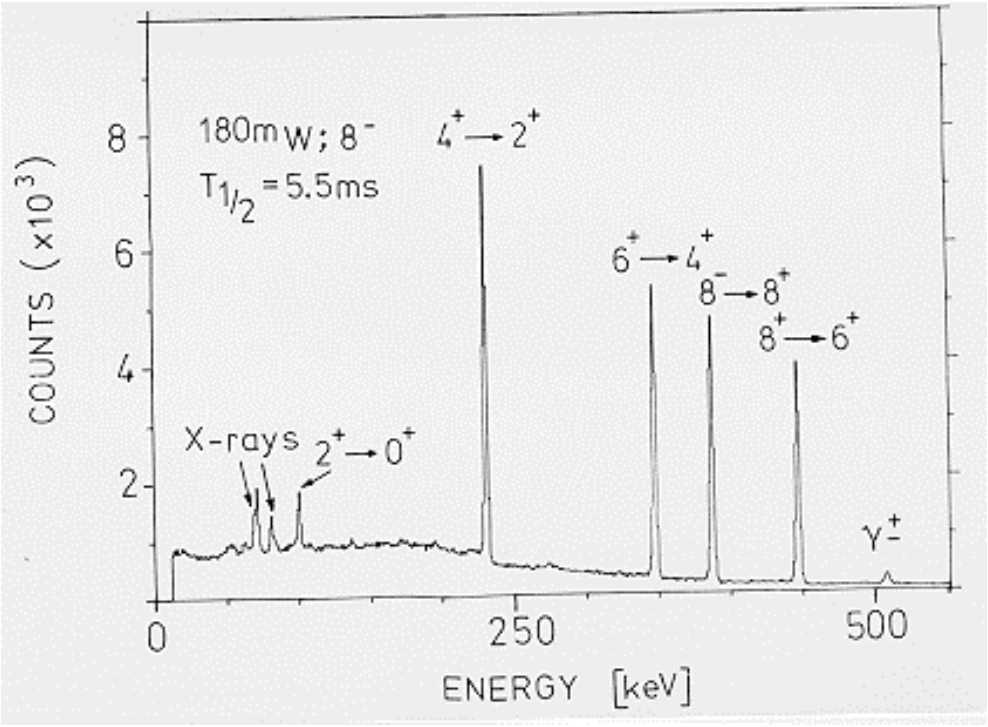

Fig. 3-26. The gamma spectrum from the decay of the mass separated 5.5ms 8^--isomer of ^{180}W produced via the 20 MeV proton + ^{nat}Ta reaction. The total running time was 30 min with 0.7 μA beam intensity in the target. [26]

The transport time (t_{tr}) in the IGISOL for all ions can be defined as being approximately equal to the evacuation time of the target chamber. On that time scale the overall efficiency begins to saturate as can be found from fig. 3-25:

$$t_{tr} \equiv t_{tc} \approx 1.5 \text{ ms}.$$

The flight time of ions through the whole ≈8 m long isotope separator system is so short, ≈10-40 μs for masses A_i= 20-200, that it does not contribute significantly to the transport time in the IGISOL.

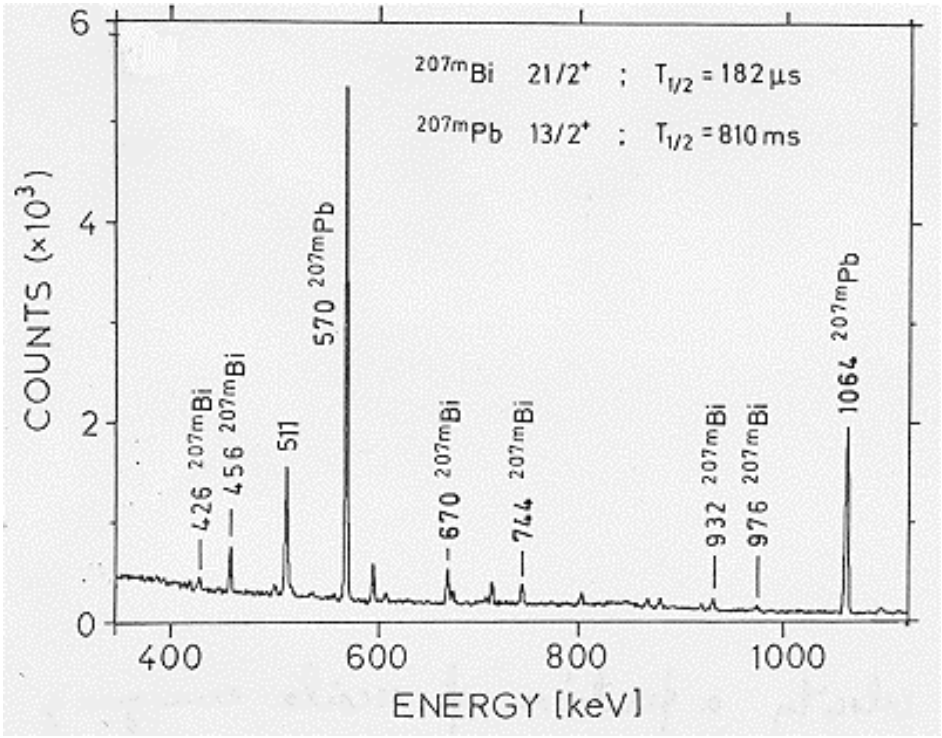

Fig. 3-27. The gamma spectrum of the recoils from the reactions ^{nat}Pb(p,pxn)^{207m}Pb and ^{nat}Pb(p,xn)^{207m}Bi at 20 MeV. [26]

The high speed and high sensitivity of the IGISOL for detecting short-lived nuclei at high spin isomeric states is demonstrated by observation of the 182 μs 21/2$^+$ isomer in ^{207}Bi (fig. 3-27). This corresponds to an angular momentum transfer of ≈>10 h, a value rather high for 20 MeV proton induced reactions.

4. SUMMARY AND DISCUSSION

The ion guide developed at the University of Jyväskylä is a device that for the first time allows primary recoil ions from nuclear reactions to be mass separated on-line. The following advantages have been reached with this method:

- very fast isotope separation; transmission time ≈>100 μs
- residence time of recoils is independent of the element
- -comparable efficiencies are obtained for volatile and nonvolatile elements
- operation at room temperature
- simple construction without wearing components
- continuously stable operation

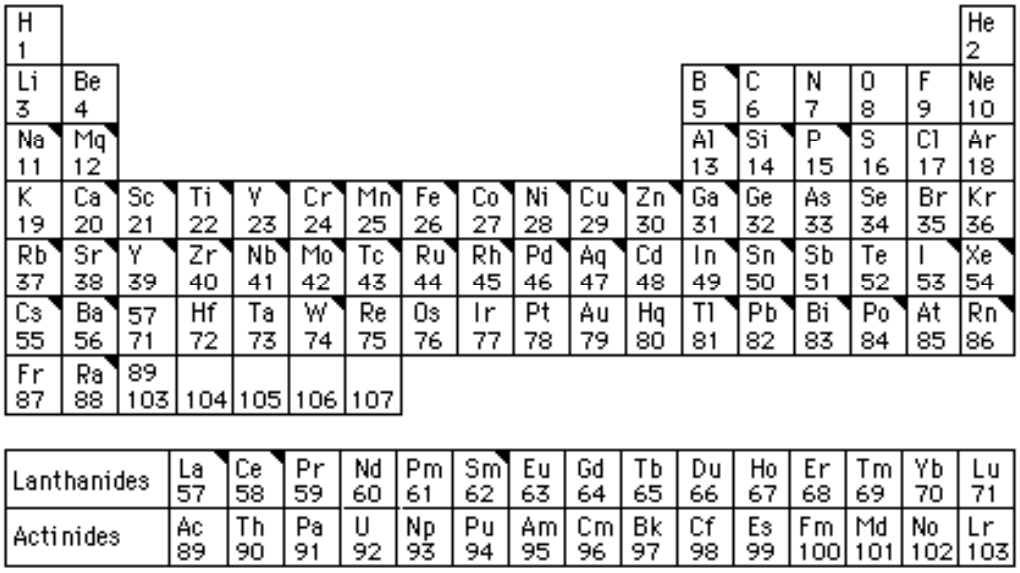

Fig. 3-28. A periodic table of the elements. Black triangles in the upper corners of the elemental characters show those elements that have been mass separated as radioactive isotopes by the ion guide isotope separator.

Presently the number of the targets used in the IGISOL experiments is 17. As a result 45 different chemical elements have been mass separated, including both volatile and very short-lived highly nonvolatile

elements like boron, yttrium, niobium and tungsten (fig. 3-28). The half-lives of the mentioned ones varied from 301 μs to 20.2 ms. Up to now the IGISOL technique has been used successfully in studies of nuclear properties of the mirror nuclei ^{47}Cr, ^{51}Fe and ^{55}Ni [112] and of the ^{45}V and ^{57}Cu [113]. Also the intruder state in ^{203}Bi was found after the IGISOL separation [114].

The ion guide was developed in three phases. The idea was first realized with a radioactive ^{227}Ac recoil source. This study taught the parameters which are important in stopping and transporting the recoil ions in flowing helium of 100-400 mbar pressure. Right from the beginning experiments showed the majority of the separated recoil ions to be atomic and +1-charged. Starting from this result an explanation was worked out for charge creation and survival processes in the ion guide. As a third phase in the investigation the ion guide separator was connected on-line to the cyclotron. Two main differences between the off- and on-line conditions are obvious: The accelerator beam of light ions produces a weak plasma in the target chamber. The initial recoil energies are usually higher in reactions.

The creation of the +1-charged recoil ions in the ion guide proceeds via several processes: Initially the recoil atoms are ionized during nuclear reactions or radioactive decays. In some cases these processes may lead to very highly charged ions. For low-energy ($\approx$<0.5 keV/u) recoils produced on the surface of the target or of the source this kind of ionization mechanism seems to be the only way to produce charged recoils. On the other hand, for recoils of higher energy emitted deep in the target, electron loss and capture processes play a central role in determining the charge of the recoils during their penetration through the target material. These processes are independent of the initial charge states produced during nuclear reactions. Recoil particles released from the target with velocities up to 0.25 v_o are thermalized in the helium volume of the ion guide. From these recoils those in the charge state +1 are likely to preserve that state during the thermalization. A fraction of neutral recoils with energies higher than 0.5 keV/u, are ionized in collisions with helium atoms.

High charge states of slow recoil ions are reset mainly in electron capture processes with helium atoms. In the case of +2-charged thermal recoil ions, the electron capture from helium atoms is improbable because of the endoergicity of such reactions. However, impurity molecules such as O_2 and N_2, can still cause notable charge transfer $+2 \rightarrow +1$. After this the capture ceases since the charge transfer $+1 \rightarrow 0$ is endoergic with He atoms and impurity molecules.

Whether the charge state +1 of the recoils will survive during the transfer out of the target chamber depends on the evacuation time of the chamber volume and on the ratio of this time to the diffusion time of the ions to the walls; in wall collisions the ions will be neutralized with high probability. During the transfer the recoils may still loose their +1-charge via three-body recombinations in helium. Especially in on-line conditions where plasma containing free electrons is present, the probability of such neutralization has to be taken into account. Such is the case when the gas pressure and projectile beam intensity are high, thus resulting in a dense plasma. When a weak radioactive source is used the latter neutralization mechanism is negligible.

In on-line conditions increasing recoil ranges enhance losses to the walls and thus reduce the overall separation efficiency. Recoils which enter helium with energies lower than 1.5 keV/u are stoppped in the gas phase. At present the overall separation efficiency is 1-10 per cent for heavy recoil ions. An interesting observation is, however, that the calculated absolute number of recoil atoms Y_d stopped in helium per unit time, unit beam intensity and unit reaction cross section, seems to be almost constant in any reaction, independent of the projectile and its energy, provided that the ion guide parameters are constant and that the target thickness exceeds the range of the recoils in the target material.

The thermalized reaction products include ions and neutral atoms. The fraction of positively charged ions among the particles has not been determined. Rough calculations indicate that the fraction of ions lost by diffusion to the walls before they leave the chamber is relatively high. Far fewer ions are estimated to be neutralized due to the weak plasma having a density of the order of 10^{-7} -10^{-6}. The yield of the positive ions at the skimmer position has been measured to be about one tenth of the

yield Y_d. Losses outside the target chamber seem to have a minor effect on the overall separation efficiency.

The use of electric fields inside the target chamber has been investigated as means of preventing ions from diffusing to the chamber walls and thereby increasing the transport efficiency and shortening the transmission time. In off-line conditions 15 -20 per cent more activity could be separated when the source was held in a positive potential. In on-line experiments no significant improvement in the yield was observed. In the latter case suitable fields are difficult to accomplish because of the plasma.

Neon, argon and nitrogen gases have been studied as alternative buffer gases, because in these gases the stopping and diffusing properties of recoils are more favourable than in helium. It turned out, however, that for recoil ions from a particular reaction the transport efficiency with helium is ten times higher than the value obtained with neon, the second best of the buffer gases. This result emphasizes the fact that inertness of the buffer gas is a key condition for survival of the ions and thus for high overall efficiency.

There is clear experimental evidence that impurity molecules in helium influence the yield. For example, it has been found that a small air leak can increase the yield. These observations suggest that it may be possible to increase the efficiency by means that are related to ionic, atomic and molecular processes inside the target chamber. This approach would probably require a high-purity gas-handling system and careful control of selected impurities.

The separation efficiency is roughly proportional to the throughput of helium through the system. The throughput can be increased either by increasing the target chamber pressure or the conductance of the chamber exit. At constant throughput the latter way increases the efficiency more rapidly, provided the target chamber pressure is $\approx>100$ mbar.

At present, the throughput cannot be increased beyond a limit set by pressure rise in the extraction chamber. This pressure rise is due to narrow pumping channels in the separator which is designed for low-pressure ion sources rather than for a high-pressure ion guide. The same

problem is inherent in all present ISOL systems that are based on the ion guide. In addition to the IGISOL in Jyväskylä and the Tohoku IGISOL [115] in Sendai, such systems are also the LIGISOL in Louvain-la-Neuve [116], Belgium and a facility at the Institute for Nuclear Study (INS) in Tokyo University [117]. The LIGISOL and the INS facility are connected to heavy-ion accelerators. The highest throughputs presently usable in on-line conditions in three of these systems are shown by blocks a in fig. 3-29.

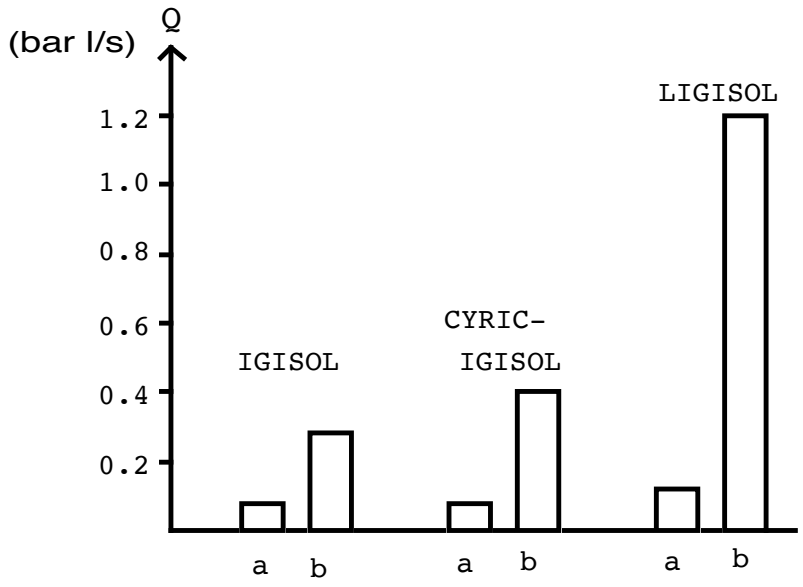

Fig. 3-29. Pumping properties of the three IGISOLs.
(a) Maximum usable helium throughput in present on-line operation.
(b) Throughput of the Roots blower at 0.5 mbar.

The problem caused by the narrow pumping channel can be solved by reconstructing the extraction chamber and its pumping unit. Then it should be possible to increase the helium throughput and with it the yield of recoil ions until the maximum throughput of the Roots blower is reached. In fig. 3-29 this limit is shown by the block b. This claim is supported by heavy ion experiments at the LIGISOL [116,118] in which increasing yields of recoil ions were observed up to the maximum throughput of the Roots blower. The ions were detected at the skimmer

position without isotope separation, and so far it was not possible to check whether the recoil ions were clustered. Up to now, however, there have been no signs that the change from atomic recoil ions to molecular ones would be abrupt with increasing pressure.

The heavy ion experiments at the LIGISOL also gave information about the plasma inside the target chamber. It was found that the total current of positive ions (mainly helium ions) emerging from the target chamber at 100 mbar pressure in the case of a heavy-ion beam is roughly equal to that observed with light projectiles as long as the electrical beam current of both projectiles is the same. This suggests that the plasma densities inside the target chamber are of the same magnitude in both cases. However, higher helium pressures create denser plasmas where negative recoil ions appear. Increasing plasma density increases the number of negative recoil ions relative to the positive ones. At 670 mbar the fractions of positive and negative recoil ions are roughly equal.

In final conclusion it is noticed that the development of the ion guide, which started with the radioactive source and then continued with light ion accelerator induced radioactivity, is now in progress at heavy-ion accelerators.

At present the IGISOLs in Jyväskylä and in Sendai are being applied in nuclear physics for study of nuclear properties of fission fragments and of mirror nuclei, respectively. In fission, although the overall efficiency of the high-energy fragments is very low (stopping efficiency $\approx<1\%$), the yields of the separated fission products are high enough for several nuclear spectroscopic applications [119,120].

In near future the development results of the IGISOLs connected to heavy-ion accelerators in Louvain-la-Neuve and in Tokyo will show whether the ion guide will prove to be the versatile universal method for isotope separation originally aimed for at the outset of the project.

REFERENCES

[1] Proceedings of the Fourth International Conference on Nuclei Far From Stability, Helsingør, 1981, CERN Report No. CERN 81-09 (unpublished).
[2] J. Äystö and J. Cerny, in Future Directions in Studies of Nuclei Far From Stability, edited by J.H. Hamilton, E.H. Spejewski, G.R. Bingham, and E.F. Zjangar (North-Holland, Amsterdam, 1980), p.257.
[3] E. Roeckl, Nucl. Phys. A400 (1983) 131c.
[4] P.G. Hansen, Annu. Rev. Nucl. Part. Sci. 29 (1979) 69.
[5] T. Björnstad et al. and the ISOLDE collaboration , Nucl. Phys. A443 (1985) 283;
P.G. Hansen and B. Jonson, Europhysics News, Vol.12, No.4 (1981) 1.
[6] Proceedings of the 10th International Conference on Electro-Magnetic Isotope Separators and Techniques Related to Their Applications, Nucl. Instr. and Meth. 186, Nos. 1,2 (1981).
[7] R. Kirchner, Nucl. Instr. and Meth. 186 (1981) 275.
[8] H. Schmeing, J.C. Hardy, E. Hagberg, W.L. Perry, J.S. Willis, J. Camplan and B. Rosenbaum, Nucl. Instr. and Meth. 186 (1981) 47.
[9] V.T. Koslowsky, D. Schardt, R. Kirchner, J. Main, D. Marx, and T. Sekine, abstract on the GSI-Scientific Report 1984, March 1985, p.100.
[10] O. Klepper, T. Batsch, S. Hoffmann, R. Kirchner, W.Kurcewicz, W. Reisdorf, E. Roeckl, D. Schardt, and G. Nyman, Z. Phys. A305 (1982) 125.
[11] J.M. Nitschke, Nucl. Instr. and Meth. in Phys. Res. A236 (1985) 1.
[12] W.-D. Schmidt-Ott, R.L. Mlekodaj, E.H. Spejewski, and H.K. Carter, Nucl. Instr. and Meth. 124 (1975) 83.
[13] J. Äystö, V. Rantala, K. Valli, M. Kortelahti, K. Eskola, and T. Raunemaa, Nucl. Instr. and Meth. 139 (1976) 325.
[14] D.M. Moltz, J. Äystö, D.M. Cable, R.D. von Dincklage, R.F. Parry, J.M. Wouters, and J. Cerny, Phys. Rev. Lett. 42 (1979) 43.
[15] A. Charvel, T. Ollivier, R. Beraud, R. Duffait, A. Emsallem, N. Idrissi, J. Genevey, and A. Gizon, Z. Phys. A321 (1985) 697.
[16] M. Brügger, N. Hildenbrand, T. Karlewski, N. Trautmann,

A.K. Mazumdar, and G. Hermann, Nucl. Instr. and Meth. in Phys. Res. A234 (1985) 218.
[17] Y. Kawase, K. Okano, and Y. Funakoshi, Nucl. Instr. and Meth. in Phys. Res. A241 (1985) 305.
[18] J. Äystö, D.M. Moltz, M.D. Cable, R.D. von Dincklage, R.F. Parry, J.M. Wouters, and J. Cerny, Phys. Lett. B82 (1979) 43.
[19] A. Ghiorso, T. Sikkeland, A.E. Larsch, and R.M. Latimer, Phys. Rev. Lett. 6 (1961) 473.
[20] J.M. Nitschke, Proc. Int. Conf. on the Properties of Nuclei Far From the Region Beta-Stability, CERN 70-30, 1 (1970) 153; H. Jungclas, R.D. Macfarlane, and Y. Fares, Phys. Rev. Lett. 27 (1971) 556.
[21] P.C. Stevenson, L.A. Cambey, and T. Smith, Arkiv Fysik 36 (1966)279; P.C. Stevenson, J.T. Larsen, and J.J. Leary, Proc. Int. Conf. on the Properties of Nuclei Far From the Region Beta-Stability, CERN 70-30, 1 (1970) 143.
[22] J. Ärje and K. Valli, Nucl. Instr. and Meth. 179 (1981) 533;
J. Ärje, J. Äystö, J. Honkanen, K. Valli, and A. Hautojärvi, Nucl. Instr. and Meth. 186 (1981) 149.
[23] J. Ärje, Phys. Scripta T3 (1983) 37.
[24] J. Ärje, J. Äystö, P. Taskinen, V. Koponen, A. Hautojärvi, K. Vierinen, and K. Valli, Proc. Int. Ion Engineering Congress, Kyoto (1983) 583.
[25] J. Ärje, J. Äystö, H. Hyvönen, P. Taskinen, V. Koponen, J. Honkanen, A. Hautojärvi, and K. Vierinen, Phys. Rev. Lett. 54 (1985) 99.
[26] J. Ärje, J. Äystö, H. Hyvönen, P. Taskinen, V. Koponen, J. Honkanen, K. Valli, A. Hautojärvi, and K. Vierinen, accepted for publication in Nucl. Instr. and Meth. in Phys. Res. A (1986).
[27] M. Yoshii, T. Shinozuka, H. Hama, T. Kamiya, and M. Fujioka, abstract on the CYRIC Annual Report 1984, p.65.
[28] J.D. Carcia, R.J. Fortner, T.M. Kawanagh, Rev. Mod. Phys.45(1973)111.
[29] D.D. Cohen and M. Harrigan, Atomic Data and Nucl. Data Tables, 33 (1985) 255.
[30] T.A. Carlsson, Phys. Rev. 130 (1963) 2361.
[31] A.H. Snell and F. Pleasonton, Phys. Rev. 100 (1955) 1396.
[32] J.S. Levinger, Phys. Rev. 90 (1953) 11.

[33] J.S. Hansen, Phys. Rev. A9 (1974) 40.
[34] A.H. Snell and F. Pleasonton, Phys. Rev. 107 (1957) 740.
[35] A.H. Snell and F. Pleasonton, Phys. Rev. 111 (1958) 1338.
[36] William Rubinson, Phys. Rev. 130 (1963) 2011.
[37] H.J. Fischbeck and M.S. Feedman, Phys. Rev. Lett. 34 (1975) 173.
[38] V. Metag, D. Habs, and H.J. Specht, Phys. Rep. 65, No.1 (1980) 1.
[39] G. Giorginis, H. Bolin, T. Faestermann, F.V. Feilitzsch, P.Kienle, C. Kozhuharov, and T. Yamazaki, Nucl. Instr. and Meth. 188 (1981) 535.
[40] K. Gunter, F. Asaro, and A.C. Helmholz, Phys. Rev. Lett. 16 (1966)362.
[41] T.A. Carlsson, W.E. Hunt, and M.O. Krause, Phys. Rev. 151 (1966) 41.
[42] W. De Wieclawik et. N. Perrin, Journald' Physique, C29 (1968) 1-104.
[43] K. Way, Internal Conversion Coefficients for Multipolarities E1,...E4, M1,...M4, Academic Press, New York and London (1973).
[44] H.D. Betz, Rev. Mod. Phys. 44 (1972) 465.
[45] H.D. Betz, Meth. of Exp. Phys. Vol.17, Academic Press (1980), pp.73-148.
[46] V.S. Nikolaev and I.S. Dmitriev, Phys. Lett. A28 (1968) 277.
[47] J. Heinemeier, P. Hvelplund, J. Ostgård Olsen, and F.R. Simpson, Phys. Scripta 10 (1974) 304.
[48] A.B. Wittkower and H.D. Betz, Phys. Rev. A7 (1973) 159.
[49] P.M. Stier, C.F. Barnett, and G.E. Evans, Phys. Rev. 96 (1954) 973.
[50] L.I. Pivovar, V.M. Tubaev, and M.T. Novikov, Sov. Ph. JETP 21 (1965) 681.
[51] T. Jorgensen, Jr., C.E. Kuyatt, W.W. Lang, D.C. Lorents, and C.A. Sautter, Phys. Rev. 140 (1965) 1481.
[52] P. Hvelplund, E. Laegsgaard, and E. Horsdal Pedersen, Nucl. Instr. and Meth. 101 (1972) 497.
[53] Proceeding of an International Symposium: Production and Physics of Highly Charged Ions, Phys. Scripta T3 (1983).
[54] H. Knudsen, H.K. Haugen, and P. Hvelplund, Phys. Rev. A23 (1981) 597.
[55] I.P. Flaks and E.S. Solo´ev, Sov.Phys.-Techn. Phys. 3 (1958) 564.

[56] J.B. Hasted and A.Y. Chong, Proc. Phys. Sov. (London) 80 (1962) 893.
[57] G.N. Ogurtsov and I.P. Flaks, Sov. Phys. JETP 15 (1962) 502.
[58] H.J. Zwally and D.W. Koopman, Phys. Rev. A2 (1970) 1851.
[59] T. Iwai, Y. Kaneko, M. Kimura, N. Kobayashi, S. Ohtani, K. Okuno, S.Takagi, H. Tawara, and S. Tsurubuchi, Phys. Rev. A26 (1982) 105.
[60] A. Müller and E. Salzborn, Phys. Lett. A62 (1977) 391, and references therein.
[61] R.E. Olson and A. Salop, Phys. Rev. A14 (1976) 579.
[62] L.P. Presnyakov and A.D. Ulantsev, Sov. J. Quant. Electron. 4 (1975) 1320.
[63] M.I. Chibisov, JETP Lett. 24 (1976) 46.
[64] E. Salzborn, Proc. Inter. Conf. on Heavy Ions Sources, Gatlinburg 1975, IEEE Trans. NS-23 (1976) 947.
[65] H.S.W. Massey, Rep. Prog. Phys. 12 (1949) 248.
[66] J.B. Hasted, Proc. Roy. Soc. A205 (1951) 421, A212 (1952) 235.
[67] D. Rapp and W.E. Francis, J. Chem. Phys. 37 (1962) 2631.
[68] L. Landau, Z.Phys. Sowjet 2 (1932) 46.
[69] C. Zener, Proc. Roy. Soc. A137 (1932) 696.
[70] E.C.G. Stueckelberg, Helv. Phys. Acta 5 (1932) 370.
[71] J.B. Hasted and A.Y.J. Chong, Proc. Phys. Soc. 80 (1962) 893.
[72] R.E. Olson, F.T. Smith, and E. Bauer, Appl. Opt. 10 (1971) 1961.
[73] W. Lindinger, Phys. Scripta T3 (1983) 115.
[74] Y. Kaneko, L.R. Megill, and J.B. Hasted, J. Chem. Phys. 45 (1966) 3741.
[75] J.F. Ziegler, Vol.5 of The Stopping and Ranges of Ions in Matter, IBM-Research, Pergamon Press Inc. (1980) USA.
[76] A. von Engel, Ionized Gases, Second Edition, Oxford University Press (1965) Great Britain.
[77] M.E. Rudd, Y.-K. Kim, D.H. Madison, J.W. Gallagher, Rev. Mod. Phys. 57 (1985) 965.
[78] Francis F. Chen, Introduction to Plasma Physics, 3.pr., New York (1977), ISBN 0-306-30755-3.
[79] Peter Rice-Evans, Spark, Streamer, Proportional and Drift Chambers, The Richelieu Press, London (1974).

[80] H.S.W. Massey, Atomic and Molecular Collisions, Taylor & Francis Ltd, London (1979), ISBN 0-85066-144-7.
[81] W.H. Kasner, W.A. Rogers, and M.A. Biondi, Phys. Rev. Lett. 7 (1961) 321.
[82] A. von Engel, Electric Plasmas: Their Nature and Uses, Taylor & Francis Ltd, London and New York (1983), ISBN 0-85066-147-1.
[83] H.J. Oskam and V.R. Mittelstadt, Phys. Rev. 132 (1963) 1445.
[84] W. Lindinger, T.D. Märk, and F. Howorka, Swarms of Ions and Electrons in Gases, Springer-Verlag Wien-New York (1984), ISBN 3-211-81823-5.
[85] M.R. Flannery, Chapter 12 in, Ionic Recombination in Atomic Processes and Applications, edited by P.G Burke and B.L. Moiseiwitsch, North-Holland Publishing Co. (1976).
[86] W. Lindinger, A.L. Schmeltekopf, and F.C. Fehsenfeld, J. Chem. Phys. 61 (1974) 2890.
[87] K.G. Spears, J. Chem. Phys. 57 (1972) 1850.
[88] I.N. Tang, M.S. Lian, and A.W. Castelmann,Jr., J. Chem. Phys. 65 (1976) 4022;
I.N. Tang and A.W. Castelmann, Jr., J. Chem. Phys. 57 (1972) 3638.
[89] Paul M. Holland and A.W. Castelmann, Jr., J. Chem. Phys. 76(8) (1982) 4195.
[90] L.C. Northcliffe and R.F. Schilling, Nucl. Data Tables A7 (1970) 233.
[91] U. Littmark and J.F. Ziegler, Vol.6 of The Stopping and Ranges of Ions in Matter, IBM-Research, Pergamon Press Inc. (1980), ISBN 0-08-023879-3.
[92] J. Lindhard, M.Scharff, and H.E. Schiøtt, Mat. Fys. Medd. Dan. Vid. Selsk. 33, No.14 (1963).
[93] H. Oetzmann, A. Feuerstein, H. Grahmann, and S. Kalbitzer, Phys. Lett. A55 (1975) 170.
[94] S. Kalbitzer, H. Oetzmann, H. Grahmann, and A. Feuerstein, Z. Phys. A278 (1976) 223.
[95] J.P. Biersack, Z. Phys. 211 (1968) 495.
[96] J. Lindhard and M. Scharff, Phys. Rev. 124 (1961) 128.
[97] Lise Bryde, N.O. Lassen, and N.O. Roy Poulsen, Mat. Fys. Medd. Dan. Vid. Selsk. 33, No.8 (1962).

[98] H.W. Ellis, R.Y. Pai, E.W. McDaniel, E.A Mason, and L.A. Viehland, Atomic Data and Nucl. Data Tables 17 (1976) 177.
[99] E.W. McDaniel and E.A. Mason, The Mobility and Diffusion of Ions in Gases, John Wiley and Sons, Inc., New York (1973).
[100] Milton Abramowitz and Irene A. Stegun, Handbook of Mathematical Functions with Formulas, Graphs, and Mathematical Tables, Dover Publications, Inc., New York (1972).
[101] G.H. Wannier, Bell System Tech. J. 32 (1953) 170.
[102] A. Roth, Vacuum Technology, North-Holland Publ. Co., (1982), ISBN 0-444-86027-4.
[103] Tilmann D. Märk and H.J. Oskam, Phys. Rev. A4 (1971) 1445.
[104] Max J. Schönhuber, IEEE Trans. on Power Apparatus and Systems, No.2 (1969) 100.
[105] J. Äystö and K. Valli, Nucl. Instr. and Meth. 111 (1973) 531.
[106] Proceedings of the Eight Intern. Conf. on Cyclotrons and Their Applications, IEEE Trans. on Nucl. Science, Vol.26, No.2 (1979).
[107] M. Fujioka, T. Shinozuka, E. Tanaka, Y. Arai, S. Hayashibe, and T. Ishimatsu, Nucl. Instr. and Meth. 186 (1981) 121.
[108] Bernard L. Cohen, Phys. Rev. 91 (1953) 74.
[109] K.A. Keller, J. Lange, H. Münzel, G. Phennig, Q-values and Excitation Functions of Nucl. Reactions, Part b, Excitation Functions for Charged-Particle Induced Nucl. Reactions edited by H. Schopper, Springer-Verlag Berlin, Heidelberg, New York 1973, ISBN 3-540-06167-3.
[110] H.W. Ellis, E.W. McDaniel, D.L. Albritton, L.A. Viehland, S.L. Lin, and E.A. Mason, Atomic Data and Nucl. Data Tables 22(3) (1978) 179.
[111] M. Blann, Report COO-3494-29, unpublished.
[112] J. Äystö, J. Ärje, V. Koponen, P. Taskinen, H. Hyvönen, A. Hautojärvi, and K. Vierinen, Phys. Lett. B138 (1984) 369.
[113] T. Shinozuka et. al., to be published.
[114] T. Lönnroth, J. Äystö, J. Ärje, J. Honkanen, V. Koponen, P. Taskinen, and H. Hyvönen, Z. Phys. A319 (1984) 149.
[115] J. Ärje, M. Yoshii, T. Shinozuka, M. Fujioka, H. Hama, T. Kamiya, and H. Takuchi, report 2.8 in JYFL Annual Report 1985.

[116] K. Deneffe, B. Brijs, M. Huyse, E. Coenen, P. van Duppen, and J. Ärje, LIGISOL: The Leuven Ion Guide Isotope Separator On-line at The Cyclone Cyclotron, I.K.S. report - November 1985.
[117] T. Nomura, report in Abstracts of the Workshop on Ion Guide Based Isotope Separation, April 9-12, 1986, in Konnevesi, Finland (unpublished).
[118] K. Deneffe, B. Brijs, M. Huyse, J. Ärje, J. Gentens, P. van Duppen, E. Coenen, and R. Coussement, report 2.9 in JYFL Annual Report 1985.
[119] H. Hyvönen, P. Taskinen, J. Honkanen, K. Valli, T. Shinozuka, J. Ärje, and J. Äystö, report 2.10 in JYFL Annual Report 1985;
[120] J. Äystö, report in Abstracts of the Workshop on Ion Guide Based Isotope Separation, April 9-12,1986, in Konnevesi, Finland (unpubl.)

APPENDICES

Commonly used symbols in alphabetical order :

A_i = mass of recoil ion [u]
A_t = mass of target atom [u]
a_o = Bohr radius = 0.529 x 10^{-8} cm
C = conductance of pumping channel [l/s]
D = diffusion coefficient [cm^2/s]
D_a = ambipolar diffusion coefficient [cm^2/s]
d = layer in target from where recoils emitted are thermalized in buffer gas [µm, µg/cm^2]
E_i = kinetic energy of recoil ion [keV]
E_P = energy of projectile beam [MeV]
h_s = height of skimmer cone [mm]
I_A = separated current of mass A [nA]
I_B = ionization potential of atom [eV]
I_P = projectile beam intensity [pµA]
I_s = ion current at skimmer position [µA]
k = Boltzmann's constant
M = molecule
n_e = electron density in buffer gas [cm^{-3}]
n_i = ion density in buffer gas [cm^{-3}]
n_n = density of buffer gas [cm^{-3}]
p_{ext} = pressure in extraction chamber of separator [mbar]
p_R = pressure at Roots blower [mbar]
p_{tc} = buffer gas pressure in target chamber [mbar]
p_{vc} = pressure in vacuum chamber [mbar]
Q = throughput of gas [mbar l/s]
q = charge state of ion
R = recoil particle
R = recoil range in buffer gas [cm, mg/cm^2]
R_t = recoil range in target [µm, mg/cm^2]
r_{tc} = radius of target chamber [cm]
S = pumping speed [l/s]

S = external electric potential in recoil chamber [V]
S_D = area of diffusion distribution
T = temperature of buffer gas [K]
T_e = electron temperature [K]
T_i = ion temperature [K]
t_f = average flow time of recoils through target chamber [s]
t_{tc} = evacuation time of target chamber ≈ residence time of recoil in
t_{tr} = transport time of ions through IGISOL [ms]
V_c = voltage between target chamber exit and collector [V]
V_d = drift velocity [cm/s]
V_{es} = voltage between target chamber exit and skimmer [V]
V_i = velocity of recoil ions in target chamber [cm/s]
V_{tc} = volume of target chamber [cm^3]
v_f = average velocity of buffer gas flow [cm/s]
v_o = Bohr velocity = 2.19 x 10^8 cm/s
x = stopping distance in target chamber [cm]
x_c = distance between target chamber exit and collector [mm]
x_{es} = distance between target chamber exit and skimmer [mm]
x_{ext} = distance between skimmer and extraction electrode [cm]
Y = yield of recoils emitted from target [s^{-1}]
Y_d = yield of recoils corresponding to layer d in target [s^{-1}]
Y^+ = yield of recoil ions [s^{-1}]
y = transport distance of recoil ions in recoil chamber [cm]
Z_i = atomic number of recoil ion
Z_t = atomic number of target atom
α_c = rate coefficient in electron transfer reaction [cm^3/s]
α_r = recombination rate coefficient [cm^3/s]
ε_o = overall efficiency
ε_{stop} = stopping efficiency of ion guide
μ = ion mobility in buffer gas [cm^2/Vs]
μ_o = reduced ion mobility [cm^2/Vs]
σ_c = electron capture cross-section [cm^2]
σ_r = nuclear reaction cross-section [cm^2]
τ_D = most probable diffusion time of ion to target chamber wall [ms]
ϕ_e = exit hole diameter [mm]

ϕ_s = skimmer hole diameter [mm]
ϕ_{ext} = hole diameter of extraction electrode [mm]

Table A : Some atomic and nuclear properties of the part of the mass separated recoils.

Reaction	E_r/A	V/v_o	q	R_t	Rp	ε_{stop}	$T_{1/2}$	Y_{ms}^+
$^{54}Fe(p,pn)^{53}Fe$	5.5	0.47	1.7	99	334	30	8.5m	570
$^{54}Fe(p,n)^{54}Co$	5.4	0.46	1.7	95	325	31	193	4700
$^{64}Zn(p,n)^{64}Ga$	3.8	0.39	1.6	79	246	41	2.6m	13800
$^{90}Zr(p,n)^{90m}Nb$	2.4	0.32	1.4	68	176	57	6.2	1400
$^{92}Mo(p,n)^{92}Tc$	1.8	0.27	1.3	52	128	78	4.4m	13000
$^{108}Cd(p,n)^{108}In$	1.2	0.22	1.1	42	90	>100	31.6m	4900
$^{181}Ta(p,2n)^{180m}W$	0.61	0.16	1.0	40	56	>100	5.5	800
$^{nat}Pb(p,x)^{207m}Bi$	0.46	0.14	0.95	37	45	>100	0.182	60
$^{11}B(d,p)^{12}B$	64	1.8	2.2	257	1630	6.1	20.2	4000
$^{24}Mg(^3He,2n)^{25}Si$	120	2.2	5.1	600	2890	3.5	218	1
$^{40}Ca(\alpha,p)^{43m}Sc$	42	1.4	4.1	500	1500	6.7	0.435	1600

E_r/A [keV/u] is the initial recoil energy, determined on the basis of conservation of linear momentum excluding the effect of the breakup of the assumed compound nucleus. **V** is the initial recoil velocity expressed relative to Bohr velocity. **q** is the calculated average charge state of the recoil ion, due to the stripping in the target. **R_t** [μg/cm^2] is the recoil range in the target and **Rp** [mbar-cm] the average range in helium. **ε_{stop}** [%] is the stopping efficiency in the target chamber. **$T_{1/2}$** [ms] is the half-life and **Y_{ms}^+** [1/μC] the mass separated number of recoil ions.

Ground plan of the cyclotron laboratory at JYFL